UNIVERSITÄT
LEIPZIG

Bachelor Thesis

Ising model on a square lattice with competing nearest and next-nearest neighbor interactions

Institut für Theoretische Physik Leipzig

Kaspar Mitte
Matrikelnummer: 3704209

Eingereicht am 17. September 2024

1. Gutachter: Prof. Dr. Wolfhard Janke
2. Gutachter: Denis Gessert

Eigenständigkeitserklärung

Hiermit erkläre ich, dass ich die vorliegende Arbeit selbstständig eigenhändig sowie ohne unerlaubte fremde Hilfe und ausschließlich unter Verwendung der aufgeführten Quellen und Hilfsmittel angefertigt habe.

Leipzig, den 17.09.2024

_____

Kaspar Mitte

Abstract

The Ising model on a square lattice with competing nearest and next-nearest neighbor interactions is highly frustrated for $J_2 = -|J_1|/2$. Further, the nature of the low temperature behavior is recently under debate. Some authors presume no phase transition at finite temperature with different kinds of correlation length divergence [1; 2]. Timmons et al. suggest a glass transition, based on computer simulation studies with a single spin update algorithm [3]. This thesis examines the mentioned presumptions by studying the specific heat and the spin autocorrelations with an alternative simulation algorithm. The studies of the specific heat with the alternative algorithm support an exponential divergence of the correlation length at zero temperature. A glassy behavior could be observed with the single spin update as well. However, it collapses for the alternative update algorithm and is perhaps a dynamic effect.

Contents

1 Introduction

A while ago, some controversies about spin glasses appeared in the condensed matter physics and statistical physics communities. Under discussion were the requirement of quenched disorder, i.e., an explicit dependence on randomness, or whether only frustration is urgently needed as it is for structural glasses. Therefore, similarities were presumed between these two kinds of glasses, turned out to be true for some systems. Further, a connection between structural glasses and regular magnetic system were closed.

A possible representative of such a system is the frustrated Ising model on a square lattice with competing nearest and next-nearest neighbor interactions. This model is subjected to significant changes of the ground-state, depending on the ratio of the nearest and next-nearest neighbor interaction. The point where these two regimes collide covers a small range around a numerical value of the interaction ratio. In this thesis, this range will be denoted as point for simplicity. Further, these regimes exhibit different kinds of ground state patterns (ferromagnetic and super-antiferromagnetic) and different kinds of phase transition (continuous and discontinuous), both regimes become continuous with enlarging distance to the point of colliding [1; 4; 5]. The nature of the low temperature phase at the colliding point remains an open question. However, it is known that at this point the system is subjected to a high frustration, i.e., it effectively freezes into a metastable state. Kalz et al. developed a simulation algorithm in particular for this case, to overcome the high frustration [1]. Timmons et al. propose the high frustration is an evidence for glassy behavior [3]. The focus of this thesis is to observe any glassy behavior with the mentioned simulation algorithm.

This work is structured as follows. Firstly, the physical background is covered from the definition of the considered model and its properties to the statistical physics treatment, Chapter 2. Chapter 3 contains all used methods for the computer simulation and the corresponding data analysis. After that, the procedure of data collection is explained and the associated data is presented and connected to the statistical physics properties, Chapter 4. Finally, the findings are summarized, and some outlooks are given in Chapter 5. The Appendix contains the implementation detail, the compiling and execution instructions and some consistency checks.

2 System under consideration

The model treated is a variation of the conventional Ising model in two dimensions with nearest neighbor interactions (NN-interactions). In this work, the next nearest neighbor interactions (NNN-interactions) are additionally considered. Therefore, the Hamiltonian is given by

$$\mathcal{H}(\boldsymbol{\sigma}) = -J_1 \sum_{\langle ij \rangle} \sigma_i \sigma_j - J_2 \sum_{[ij]} \sigma_i \sigma_j, \tag{1}$$

where $\boldsymbol{\sigma} \in \{-1, 1\}^N$ denotes the microstate with N spins, σ_i the components of $\boldsymbol{\sigma}$, $J_1 > 0, J_2 < 0$ are coupling constants, $\langle ij \rangle$ denotes the NN-interactions and $[ij]$ the NNN-interactions. The studies in this thesis are limited to square lattices with periodic boundary conditions, therefore the total number of spins in a system with the lattice length L is $N = L^2$.

2.1 Ground-state properties

During the discussion of the ground-state properties of the system described above, Timmons et al. refer in their work [3] to a paper of Fan and Wu [6] from 1969, containing quite a general analysis of ground-state properties of the vertex model for different cases. They mention that for $J_2 \in (-J_1/2, 0]$, the system has a ferromagnetic ground-state, i.e., that all σ_i are either $+1$ or -1. To determine the ground-state energy consider the left lattice in Figure 2.1. Each

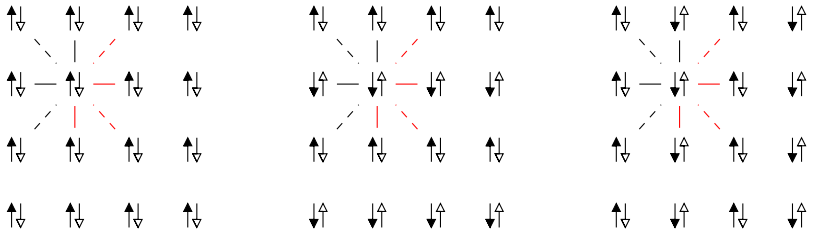

Figure 2.1: The sketch shows the possible ground-state patterns (left) for $J_2 \in (-J_1/2, 0]$, (middle) and (right) for $J_2 \in (-\infty, -J_1/2)$. The solid lines represent the NN-interactions and the dashed ones the NNN-interactions.

bond drawn contributes ± 1 to the sums in the Hamiltonian (1), they all are $+1$ in the case depicted. To avoid double summations, sum only over the bonds drawn red for each lattice site. Therefore, one obtains the ground-state energy

through a summation over the whole lattice

$$E_0 = \sum_{i=1}^{N} (-J_1 \cdot 2 - J_2 \cdot 2) = -2N(J_1 + J_2).$$

For $J_2 \in (-\infty, -J_1/2)$, the system has a super-antiferromagnetic ground-state [3]. Thus, the spins order in striped patterns of alternating spin values, shown in Figure 2.1 (middle and right lattice). The ground-state energy of these four possible states can be computed analogously to the previous case, with the difference that the NN-interactions cancel out for each lattice site. Hence, the ground-state energy is given by

$$E_0 = \sum_{i=1}^{N} (-J_1 \cdot (1-1) - J_2 \cdot (-2)) = 2NJ_2.$$

Comparing these two ground-state energies, one obtains a special case for $J_2 = -\frac{J_1}{2}$ because then, the two energy-levels coincide. This value of J_2 separates these two ground-state regimes, called in the following critical point. At the critical point, the system has more than the six ground-states of Figure 2.1. To obtain the other ground-states, regard the sketches in Figure 2.2. Flipping the highlighted lines of aligned spins in the sketched environment, the energy of the system does not change. To see that, let $E_{\text{new/old}}$ be the part of the energy,

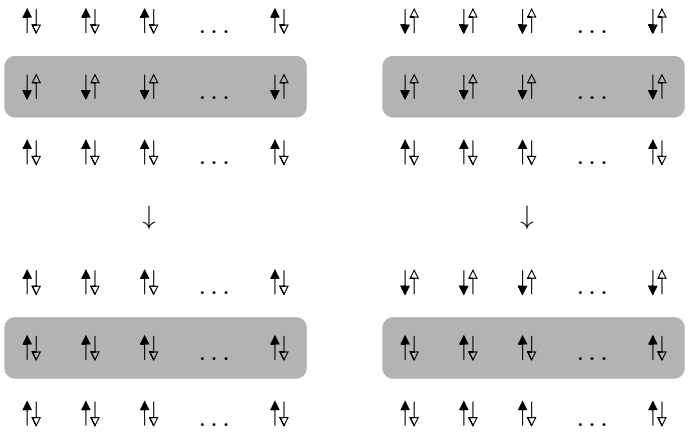

Figure 2.2: The sections of horizontal ground-state patterns for the system at the critical point are depicted. The highlighted rows correspond to the lines that are getting flipped.

the highlighted line contributes to. For the left sketch in Figure 2.2

$$\begin{aligned} E_{\text{new}} - E_{\text{old}} &= (-J_1 L \cdot (2-2) - J_2 L \cdot (-4)) - (-J_1 L \cdot 4 - J_2 L \cdot 4) \\ &= -2J_1 L - (-2J_1 L) = 0 \end{aligned}$$

holds. For the right graphic one obtains

$$\begin{aligned} E_{\text{new}} - E_{\text{old}} &= (-J_1 L \cdot (3-1) - J_2 L \cdot (2-2)) - (-J_1 L \cdot (3-1) - J_2 L \cdot (2-2)) \\ &= -2J_1 L - (-2J_1 L) = 0. \end{aligned}$$

Hence, the two processes do not change the energy of the system and one can construct with these two line flips a total of 2^L other ground-states. For the vertical pattern one can construct in an analogous way 2^L ground-states, as well. Both cases contain the ferromagnetic ground-states, therefore the total number of ground-states generated has to be subtracted by 2, finally leading to a degeneracy of $2^{L+1}-2$ [1].

2.2 Statistical physics treatment

In this work the system under consideration is coupled with the environment through an exchange of energy, but not of particles. Hence, the statistical equilibrium properties of the microstates can be described by the canonical ensemble, i.e., $\boldsymbol{\sigma}$ occurs at an environment temperature T with a probability

$$P(\boldsymbol{\sigma}) = Z_T^{-1} \exp\left(-\frac{\mathcal{H}(\boldsymbol{\sigma})}{kT}\right). \tag{2}$$

where $Z_T{=}\sum_{\boldsymbol{\sigma}} \exp(-\mathcal{H}(\boldsymbol{\sigma})/kT)$ denotes the partition function and k the Boltzmann constant. Therefore, the expectation value of an arbitrary observable $\mathcal{O}$ depends only on the temperature T and its thermodynamic expectation value can be computed by

$$\langle \mathcal{O} \rangle = \sum_{\boldsymbol{\sigma}} \mathcal{O}(\boldsymbol{\sigma}) P(\boldsymbol{\sigma}).$$

The equilibrium treatment through the canonical ensemble requires the ergodicity, i.e., the expectation value $\langle \mathcal{O} \rangle_{\text{time}}$ obtained through the time evolution of the system coincides with $\langle \mathcal{O} \rangle_{\text{phase space}}$ received through the geometry of the phase space (Ergodic Theorem), in particular its energy surface. Or in more ingenuous words, the system reaches every microstate on the energy surface within a sufficiently long duration. [7; 8] Therefore, Equation (2) describes only the thermodynamic equilibrium where the probabilities are independent of the trajectory in the phase space, which in general is not always the case.

Performing the summation over all possible microstates $\sum_{\boldsymbol{\sigma}}$ is generally difficult in practice. The density of states delivers a concept, to overcome this difficulty. For explanation, let's consider the possible eigenvalues of the Hamiltonian $E = \mathcal{H}(\boldsymbol{\sigma})$ and the possible eigenvalues of a microstate dependent observable $M = \mathcal{M}(\boldsymbol{\sigma})$. The density of states $\Omega(E, M)$ assigns the number of corresponding microstates to the values E and M. The expectation value of observables depending on E and M, can then be rewritten as

$$\langle \mathcal{O} \rangle = Z_T^{-1} \sum_{E,M} \mathcal{O}(E, M) \Omega(E, M) \exp\left(-\frac{E}{kT}\right).$$

Thus, the observable implicitly depends on the microstates $\boldsymbol{\sigma}$. To avoid handling with a density of states depending on E and M, a dependency reduction can be performed through $\Omega(E) = \sum_M \Omega(E, M)$. To compute the above expectation value, an effective energy dependent observable is necessary, received by

$$\begin{aligned}\langle \mathcal{O} \rangle &= Z_T^{-1} \sum_E \frac{\sum_M \mathcal{O}(E, M)\Omega(E, M)}{\sum_M \Omega(E, M)} \Omega(E) \exp\left(-\frac{E}{kT}\right) \\ &= Z_T^{-1} \sum_E \mathcal{O}_{\text{eff}}(E)\Omega(E) \exp\left(-\frac{E}{kT}\right). \end{aligned} \tag{3}$$

The effective observable $\mathcal{O}_{\text{eff}}(E)$ is also known as list, an actual energy dependency of $\mathcal{O}(E, M)$ is not required. Further, $\mathcal{O}_{\text{eff}}(E)$ is the expectation value of $\mathcal{O}(\boldsymbol{\sigma})$ with $\boldsymbol{\sigma}$ distributed according to the micro canonical ensemble (no E exchange). This reduction procedure works with any observable M. [9]

Thermodynamic quantities

To treat the studied thermodynamic quantities properly, consider the Hamiltonian (1) with a non-vanishing external magnetic field h aligned parallelly to the spins σ_i

$$\mathcal{H}_h(\boldsymbol{\sigma}) = -J_1 \sum_{\langle ij \rangle} \sigma_i \sigma_j - J_2 \sum_{[ij]} \sigma_i \sigma_j + h \sum_{i=1}^{N} \sigma_i.$$

For simplicity, let $\mathcal{M}(\boldsymbol{\sigma})$ denotes the microstate dependent sum $\sum_{i=1}^{N} \sigma_i$. Using the modified Hamiltonian, define the thermodynamic potential

$$F(T, h) = -kT \ln\left(Z_{T,h}\right) = -kT \ln\left(\sum_{\boldsymbol{\sigma}} \exp(-\mathcal{H}_h(\boldsymbol{\sigma})/kT)\right), \tag{4}$$

also known as canonical free energy. Its partial derivatives are given by

$$\begin{aligned}\partial_T F(T, h) &= -k \ln\left(Z_{T,h}\right) - \frac{kT}{Z_{T,h}} \sum_{\boldsymbol{\sigma}} \frac{\mathcal{H}_h(\boldsymbol{\sigma})}{kT^2} \exp\left(-\frac{\mathcal{H}_h(\boldsymbol{\sigma})}{kT}\right) \\ &= -k \ln\left(Z_{T,h}\right) - \frac{\langle E \rangle}{T} \end{aligned} \tag{5}$$

$$\begin{aligned}\partial_h F(T, h) &= \frac{kT}{Z_{T,h}} \sum_{\boldsymbol{\sigma}} \frac{\partial_h \left(\mathcal{H}(\boldsymbol{\sigma}) + h\mathcal{M}(\boldsymbol{\sigma})\right)}{kT} \exp\left(-\frac{\mathcal{H}_h(\boldsymbol{\sigma})}{kT}\right) \\ &= -\langle M \rangle, \end{aligned} \tag{6}$$

where the non-respected macroscopic state variables are kept fixed. Especially, both the internal energy $\langle E \rangle$ and the conventional magnetization[1] $\langle M \rangle$ can be

[1] The term conventional is used, because some modified magnetizations are defined in the following.

obtained through partial derivatives of the free energy F. Furthermore, the internal energy is a function received via a Legendre-transformation [8, p.79] of the free energy, i.e., $\langle E\rangle(\partial_T F, h) = T\partial_T F(T,h) - F(T,h)$. Other relevant thermodynamic quantities are the specific heat c_V and susceptibility χ defined as the second partial derivatives of the free energy

$$\begin{aligned} c_V &= -\frac{T\partial_T^2 F(T,h)}{N} = \frac{T}{N}\left(-\frac{k}{Z_{T,h}}\sum_{\boldsymbol{\sigma}}\frac{\mathcal{H}_h(\boldsymbol{\sigma})}{kT^2}\exp\left(-\frac{\mathcal{H}_h(\boldsymbol{\sigma})}{kT}\right) + \frac{\langle E\rangle}{T^2} + \frac{\partial_T\langle E\rangle}{T}\right) \\ &= \frac{\sum_{\boldsymbol{\sigma}}\mathcal{H}_h(\boldsymbol{\sigma})\partial_T\exp\left(-\mathcal{H}_h(\boldsymbol{\sigma})/kT\right)}{NZ_{T,h}} - \frac{\langle E\rangle\sum_{\boldsymbol{\sigma}}\partial_T\exp\left(-\mathcal{H}_h(\boldsymbol{\sigma})/kT\right)}{NZ_{T,h}} \\ &= \frac{\langle E^2\rangle - \langle E\rangle^2}{NkT^2} \end{aligned} \tag{7}$$

$$\begin{aligned} \chi &= -\frac{\partial_h^2 F(T,h)}{N} = \frac{\partial_h\langle M\rangle}{N} \\ &= \frac{\sum_{\boldsymbol{\sigma}}\mathcal{M}(\boldsymbol{\sigma})\partial_h\exp\left(-\mathcal{H}_h(\boldsymbol{\sigma})/kT\right)}{NZ_{T,h}} - \frac{\langle M\rangle\sum_{\boldsymbol{\sigma}}\partial_h\exp\left(-\mathcal{H}_h(\boldsymbol{\sigma})/kT\right)}{NZ_{T,h}} \\ &= \frac{\langle M^2\rangle - \langle M\rangle^2}{NkT}. \end{aligned} \tag{8}$$

Therefore, the internal energy, conventional magnetization, specific heat and susceptibility can be expressed both in terms of partial derivatives of a thermodynamic potential and in terms of expectation values. This fact justifies the importance of these observables for critical phenomena studies with computer simulations. [8]

The quantities above are these for a non-vanishing external field. Taking the limit $\lim_{h\to 0}\mathcal{O}$ corresponding to $\mathcal{H}_h, Z_{T,h} \to \mathcal{H}, Z_T$, the quantities are obtained for $h=0$.

2.3 Phase transition

In thermodynamics there exists critical phenomena so-called phase transitions, where the system is subjected to significant property changes. Such transitions occur through changes in the symmetry of the system, i.e., changes to a state of more (or less) symmetry or changes between different unrelated symmetries [7]. The different states are called phases, the state with the lower symmetry is named ordered phase, as opposed to the disordered phase of higher symmetry. The engine of such transitions are variations of the macroscopic state variables. In the considered case these are the temperature T and the external magnetic field h. To describe these phenomena quantitatively, an order parameter is commonly used, assigning to the ordered phase a finite value and vanishing for the disordered one. More generally, the order parameter is finite at one of the phases and vanishes at the other one, but such an order parameter does not always exist. [7; 8]

For the system under consideration, a quantity of high interest is the two point spin correlation function

$$G(i,t_1,j,t_2) = \langle \sigma_i(t_1)\sigma_j(t_2)\rangle - \langle \sigma_i(t_1)\rangle\langle \sigma_j(t_2)\rangle,$$

where t_1, t_2 denotes two times in system history. To achieve a better understanding of this function, let's consider the term $1+\langle \sigma_i(t_1)\sigma_j(t_2)\rangle$, which is proportional to the probability of observing the i^{th} spin at t_1 aligned equally to the j^{th} spin at t_2 [10]. Hence, this correlation function evaluates the microscopic relations of the system so $G(i,t_1,j,t_2)$ quantifies the correlations between $\sigma_i(t_1)$ and $\sigma_j(t_2)$. The considered system has translation invariance, therefore G is actually a function of the delay $j-i$. Two cases can be examined, firstly, at $t_1=t_2$, the two point spin correlation function decays exponentially for large delays $j-i \gg 1$ according to

$$G(j-i) \propto |a\cdot(j-i)|^{-\kappa} \exp\left(-\frac{a\cdot(j-i)}{\xi}\right),$$

with the lattice constant a, a dimension and system dependent exponent κ and the spatial correlation length ξ modelling the effective affecting range of a spin [9]. Secondly, for $j-i=0$, it is convenient to average the spin values over the whole lattice, because no lattice site is preferable under periodic boundary condition. Furthermore, to normalize the resulting expression to unity for $t_1=t_2$ and afterward to take the thermodynamic expectation value. Thus, the general expression of the two point spin correlation function becomes

$$\begin{aligned} G(t_1,t_2) &= \left\langle \frac{\frac{1}{N}\sum_{i=1}^{N}\sigma_i(t_1)\sigma_i(t_2) - \frac{1}{N}\sum_{i=1}^{N}\sigma_i(t_1)\cdot\frac{1}{N}\sum_{i=1}^{N}\sigma_i(t_2)}{1-\frac{1}{N}\sum_{i=1}^{N}\sigma_i(t_1)\cdot\frac{1}{N}\sum_{i=1}^{N}\sigma_i(t_2)} \right\rangle \\ &= \left\langle \frac{N\sum_{i=1}^{N}\sigma_i(t_1)\sigma_i(t_2) - \mathcal{M}(\boldsymbol{\sigma}(t_1))\mathcal{M}(\boldsymbol{\sigma}(t_2))}{N^2 - \mathcal{M}(\boldsymbol{\sigma}(t_1))\mathcal{M}(\boldsymbol{\sigma}(t_2))} \right\rangle. \end{aligned} \tag{9}$$

In a mathematical sense, the free energy $F(T,h)$ is a non-analytical function at the phase transition. Hence, phase transitions can be characterized according to the discontinuities of the partial derivatives of $F(T,h)$. A phase transition is called discontinuous if $F(T,h)$ is continuous and at least one of the first derivatives has a discontinuity. A continuous phase transition is classified through a continuous first partial derivatives and singularities or discontinuities in the higher order. [8] Of course there are some exotic cases, which cannot be classified in a conventional fashion. It should be emphasized that these discontinuities and singularities actually appear for infinite system sizes only in the thermodynamic limit. For finite systems the free energy is usually analytical. Only finite system sizes are possible in computer simulation studies. Therefore, the results have to be extrapolated to $N\to\infty$. [9]

In the following, the conventional kinds of phase transitions are shortly described, as well as a representative of the exotic ones. Additionally, the discussions are limited to the temperature driven phase transitions. Thus, the phase transition point is located through a critical temperature T_c.

Discontinuous phase transition

As mentioned, this kind of phase transitions are characterized by discontinuous changes of the first partial derivative of the free energy. Hence, discontinuities in the entropy $S = -\partial_T F(T,h)$ or magnetization $\langle M \rangle = -\partial_h F(T,h)$ suggest δ-function singularities of the specific heat or the susceptibility. The free energy is reflected by two different analytical functions $F_1(T,h)$ for $T < T_c$ and $F_2(T,h)$ for $T > T_c$, satisfying the continuity condition $F_1(T_c,h) = F_2(T_c,h)$ at the transition point. Each function corresponds to a phase [7]. Thus, the transition point exhibits a coexisting state of both phases, implying a finite spatial correlation length ξ, i.e., there are finite regions corresponding to the phases involved. In simulation studies, such phenomena are noticeable by double-peaked energy or magnetization histograms, where each peak corresponds to one of the phases. [11]

The considered system is subjected to a discontinuous phase transition for $J_2/J_1 \in (-g^*, -1/2)$ with $g^* \approx 0.67$ [4], which is still under debate. This critical behavior is supported by the work of Kalz et al. [1] as well. Especially, they obtain the double-peaked histograms and argue for a δ-function singularity of the specific heat in the thermodynamic limit. For this case, the ground-states are super-antiferromagnetic as pointed out in Section 2.1. This justifies the following choice of the order parameter

$$\mathcal{M}_s(\boldsymbol{\sigma}) = \begin{cases} \mathcal{M}_h(\boldsymbol{\sigma}) = \sum_{i=1}^{N} (-1)^{x_i} \sigma_i & \text{for } |\mathcal{M}_h| > |\mathcal{M}_v| \\ \mathcal{M}_v(\boldsymbol{\sigma}) = \sum_{i=1}^{N} (-1)^{y_i} \sigma_i & \text{for } |\mathcal{M}_h| \leq |\mathcal{M}_v| \end{cases} \tag{10}$$

where $x_i, y_i \in \{1, ..., L\}$ index the columns and rows of the lattice. $\mathcal{M}_s$ assigns the super-antiferromagnetic ground-states with $\pm N$ and effectively vanishes for spin configurations distributed uniformly (corresponding to the high temperature phase). Furthermore, $\langle M_{s,h,v} \rangle$ can be considered as modified magnetizations and all previous expressions of quantities containing the conventional magnetization can be adjusted by replacing $\mathcal{M}$ with $\mathcal{M}_{s,h,v}$, like Equations (8) and (9). In the following, the index s, h, v is related to this very replacement.

Continuous phase transition

The phase transitions of continuous kind have at least continuous changes of the free energy and their first partial derivatives. The ones being discontinuous in their second derivatives in form of singularities have a major status and are being examined in the following. The corresponding free energy can be expressed by a single continuously differentiable function describing both phases. Therefore, the transition point exhibits a continuous mixture containing the symmetries of both phases, i.e., there is no coexisting of finite regions corresponding to the different phases and rather a single "transition phase" subjected to the whole system. [7; 8] Hence, the spatial correlation length diverges $\xi \to \infty$ at T_c, according to the power law

$$\xi \propto |1 - T/T_c|^{-\nu} + \Delta_\xi,$$

where ν denotes a characteristic exponent also known as the critical exponent and Δ_ξ is a correction term. The singularities of the second partial derivatives of $F(T,h)$ and the order parameter (for the magnetic systems, $\langle M \rangle$) behaves according to power laws in the vicinity of T_c as well,

$$c \propto |1 - T/T_c|^{-\alpha} + \Delta_c,$$

$$\langle M \rangle \propto (1 - T/T_c)^{\beta} + \Delta_M \quad \text{for} \quad T < T_c,$$

$$\chi \propto |1 - T/T_c|^{-\gamma} + \Delta_\chi,$$

with the critical exponents α, β, γ and the correction terms $\Delta_{(\cdot)}$. [9] The possible values of the exponents $\alpha, \beta, \gamma, \nu$ define the universality of critical phenomena, i.e., in proximity of T_c, the microscopic details of the interactions becomes irrelevant and only universal properties, like dimension, symmetry of the order parameter or general character of the interaction are essential. Therefore, different systems with the same universal properties behave equally in the vicinity of T_c. These facts are supported by the renormalization group theory. [8] In computer simulation studies, it is impossible to observe actual divergences, because only finite system sizes are possible such that the singularities appear rather as dislocated and rounded peaks, and it is necessary to extrapolate the finite size observations to an infinite system size (thermodynamic limit). This can be done with the finite-size scaling approach $\xi \to L$, where L is the linear system size (lattice length), implying the relation

$$|1 - T/T_c| \propto L^{-1/\nu}. \tag{11}$$

For finite systems the spatial correlation length is limited by L, justifying the replacement of ξ with large L. [9]

The discussion above holds for a huge number of systems but in some cases the phase transition exhibits a continuous character and a different spatial correlation length divergence, i.e., the power law divergence of ξ is not strong enough, causing an exponential divergence

$$\xi \propto \exp\left(c\,|1 - T/T_c|^{-\overline{\nu}}\right) + \Delta_\xi,$$

with some system dependent constant c and a new exponent $\overline{\nu}$. Similarly, the finite-size approach can be followed according to the replacement of ξ with large L/L_0, leading to the relation

$$|1 - T/T_c| \propto \left(\ln\left(L/L_0\right)\right)^{-1/\overline{\nu}}, \tag{12}$$

with a system dependent characteristic length scale L_0. This idea is originated by a work of Kosterlitz [12], studying the two-dimensional XY-model ($\overline{\nu} = 1/2$).

Back to the considered system of this thesis, different papers [1; 13; 14] point out that the kind of the phase transition is continuous for the system with $J_2/J_1 \in (-1/2, 0]$. The corresponding order parameter is the conventional

magnetization $\mathcal{M}(\boldsymbol{\sigma})$. Furthermore, they found the same set of critical exponents as the conventional Ising model ($J_2/J_1 = 0$), suggesting a membership of the Ising universality class. Hence, all mentioned variations of the considered system behave equally in proximity of there respective transition point. It should be emphasized that the critical exponents are equal but the transition temperatures T_c differ.

Glassy phase transition

These kinds of phase transition are subjects of recent researches. There are dynamical and static approaches to treat these phase transitions in the context of statistical physics. In the low temperature phase, the difficulty of this kind originates from the non-ergodic behavior and the huge number of deep free energy valleys (metastable states), i.e., the system is easily trapped in a sub-state space and effectively freezes in this state. Especially, the states minimizing the free energy in the state space have a random character, thus the corresponding microstates have no significant similarities and appear disordered or asymmetrical (no ordered patterns in a conventional sense such as the ferromagnetic or superantiferromagnetic ones). Usually, the freezing into a metastable state results from competing interactions. Conventionally, the term "glassy" is distinguished in spin glasses and structural glasses. [15; 16]

A spin glass is commonly characterized by freezing into a metastable state and quenched disorder, i.e., the system depends explicitly on random variables that are independent of time on all experimental time scales [15]. In context of spin glasses the freezing property is also known as frustration. The latter property can be explained by the Edwards-Anderson model defined as the Hamiltonian

$$\mathcal{H}(\boldsymbol{\sigma}) = -\sum_{\langle ij \rangle} J_{ij}\sigma_i\sigma_j,$$

with Gaussian-distributed J_{ij}. The thermodynamic quantities of interest are obtained through their averages over different system realizations corresponding to a set of J_{ij} drawn randomly, also known as replica. Hence, the disordered appearance of the metastable states or "random-valleys" in the free energy results from explicit random variables in the Hamiltonian. [15] However, some newer publications, like Ref. [17; 18], argue for spin glass without quenched disorder, i.e., self generated randomness.

A structural glass effectively freezes into an unsymmetrical microstate as well, denoted in this context as an amorphous state. However, their origin is different, the randomness or disorder of the metastable states is self generated like the arrangement of the atomic bonds in chemical glass. Therefore, the "random-valleys" characteristic of the free energy is a system related property and less artificial than in spin glasses, i.e., the main difference to spin glasses is the absence of quenched disorder. Thus, the replicas result from independent system preparations and not from a new set of random variables. [16]

Kirkpatrick et al. begin to blur the boundaries between spin glasses and structural glasses in their papers [19; 20], mentioning analogies between structural glasses and Potts spin glasses. They list similarities to discontinuous phase transitions and suggest possible glassy behavior of frustrated regular spin problems. Furthermore, these kinds of problems are named discontinuous spin glasses, which exhibits a continuous change of the entropy, internal energy and a discontinuous change of the order parameter [16]. A general theory containing these kinds of problems is developed in a paper of Westfahl et al. [17].

This analytical approach predicts a possible temperature range of the glass transition temperature T_g, where the system effectively freezes into a metastable state, i.e., $T_g \in (T_K, T_A)$ with the limit temperatures T_K, T_A of glassy behavior. Mézard et al. [16] mention a relaxation time τ divergence of the spin autocorrelations at T_g where the explicit value of this temperature depends on the cooling rate [17]. The lower boundary T_K corresponds to the ideal glass transition temperature in the infinite cooling rate limit [3]. A connection between τ and the limit temperature T_K is given by the Vogel-Fulcher law [20; 17]

$$\tau \propto \exp\left(\frac{c \cdot T_K}{T - T_K}\right). \tag{13}$$

The upper boundary T_A exhibits the occurrence temperature of the metastable state [20], i.e., these states appear with a non-negligible probability, resulting in significantly increasing spin autocorrelations, because the system is subjected to strong memory effects.

The nature of the system under consideration for $J_2/J_1 = -1/2$ is unclear in the low temperature range (nonzero T). There are some evidence supporting a glassy behavior depicted above [3]. Firstly, the huge number of metastable states (degeneracy), Section 2.1 and the frustration arising from the competition between the NN-term and repulsive NNN-term in the Hamiltonian (1). Secondly, discontinuous spin glasses have both a continuous and discontinuous character, which may connect the two regimes for $J_2/J_1 \in (-g^*, -1/2)$ and $J_2/J_1 \in (-1/2, 0]$. However, there are also evidences against it, like the absence of the random or disordered characteristic of the metastable states, and especially the ordered form of the ground-states [1; 2].

3 Methods

3.1 Monte Carlo simulations

In a statistical physic setup, simulation methods become important either if the enumeration of the microstates reaches a huge number of terms or if there is no analytical method to determine the density of states or partition function of the considered system. To overcome these problems, sample the time evolution of the system with fixed macroscopic state variables, i.e., a fixed environment temperature T for the canonical ensemble. Hence, the microstates arising should be distributed according to the probability distribution of the canonical ensemble, Equation (2), (if the system is in equilibrium) and one estimates the expectation value through the given microstates $\boldsymbol{\sigma}_k$ where k indexes the M measurements. Therefore, an arbitrary observable $\mathcal{O}$ can be estimated by

$$\hat{\mathcal{O}}_T = \frac{1}{M} \sum_{k=1}^{M} \mathcal{O}(\boldsymbol{\sigma}_k) \tag{14}$$

if M is sufficiently large and the system is properly equilibrated, i.e., the occurrence of the microstates follows the underlying probability distribution. To achieve such time evolution of the microstates one can use Markow chain Monte Carlo methods (MCMC methods) originating from the work of Metropolis et al. [21].

MCMC method

The idea of MCMC methods is to let the system transit from a microstate $\boldsymbol{\sigma}_i$ to $\boldsymbol{\sigma}_j$ with a transition probability W_{ij}, and thus the transition $\boldsymbol{\sigma}_i \to \boldsymbol{\sigma}_j$ happens with a probability W_{ij} where the case $i = j$ is allowed as well. To sample the underlying distribution, the following requirements for W_{ij} are necessary

$$W_{ij} \geq 0 \qquad \forall i, j \tag{15}$$

$$\sum_j W_{ij} = 1 \qquad \forall i \tag{16}$$

$$W_{ij} P(\boldsymbol{\sigma}_i) = W_{ji} P(\boldsymbol{\sigma}_j) \qquad \forall i, j \tag{17}$$

$$\exists \boldsymbol{\sigma}_{k_1}, ..., \boldsymbol{\sigma}_{k_n} \; n \in \mathbb{N} \;\text{ such that } \sum_{k_1,...,k_n} W_{ik_1} \cdot ... \cdot W_{k_n j} > 0 \qquad \forall i, j. \tag{18}$$

Conditions (15) and (16) ensure the strict positivity and normalization of probabilities. Equation (17) is also known as detailed balance, implying that a transition $\boldsymbol{\sigma}_i \to \boldsymbol{\sigma}_j$ is reversible, and hence no directions of the transitions

$\boldsymbol{\sigma}_i \leftrightarrow \boldsymbol{\sigma}_j$ is preferred. The balance condition $\sum_i W_{ij} P(\boldsymbol{\sigma}_i) = P(\boldsymbol{\sigma}_j)$ can easily be obtained by a summation of the detailed balance from which it follows that the equilibrium probabilities $P(\boldsymbol{\sigma}_j)$ are the components of an eigenvector of the transition matrix (W_{ij} can be considered as a matrix). Therefore, the transitions conserve the underlying equilibrium distribution, and it is urgently necessary to equilibrate the system such that the occurrence of the microstates reflects the equilibrium distribution. Condition (18) ensures the ergodicity, i.e., all possible states can be reached through a finite number of transitions with non-vanishing probability. Thus, no transition traps the system in a sub-state space. [9]

In this thesis, all microstate transitions are constructed via the following steps. Firstly, one selects a transition proposal from $\boldsymbol{\sigma}_i$ to $\boldsymbol{\sigma}_j$ with probability f_{ij}. Secondly, the transition is accepted with a probability w_{ij}. Hence, for $i \neq j$, the transition probability is given by $W_{ij} = f_{ij} w_{ij}$ and by $W_{ii} = 1 - \sum_{n \neq m} W_{nm}$ for $i = j$. The acceptance probability

$$w_{ij} = \min\left\{1, \frac{f_{ji} P(\boldsymbol{\sigma}_j)}{f_{ij} P(\boldsymbol{\sigma}_i)}\right\} = \min\left\{1, \frac{f_{ij}}{f_{ji}} \exp\left(-\frac{\mathcal{H}(\boldsymbol{\sigma}_j) - \mathcal{H}(\boldsymbol{\sigma}_i)}{kT}\right)\right\}$$

then defines the Metropolis algorithm, which indeed satisfies Condition (15), (16) and (17). [9]

The ergodicity condition depends on the exact shape of the microstate changing rule. For the numerical work the following two local update algorithms are implemented.

Single spin update algorithm

In this update method the transition $\boldsymbol{\sigma}_i$ to $\boldsymbol{\sigma}_j$ results from a single spin flip obviously satisfying Condition (18) because each possible state can be generated by a finite number of spin flips. Firstly, one chooses a spin at random corresponding to $f_{ij} = 1/N$. Secondly, this spin will be flipped with a probability $w_{ij} = \min\{1, \exp(-\Delta E/kT)\}$, where ΔE denotes the energy deviation resulting from flipping the spin. The simulation steps are conventionally measured in sweeps, where one sweep contains N spin flip proposals.

The advantage of this compact algorithm is that a huge number of systems can be simulated because a single spin flip can easily be applied to any "Ising like" system. However, for frustrated systems at low T the proposals are almost certainly refused and a transition between the free energy minima requires a relatively huge number of accepted proposals, thus the system remains in the current microstate over a large number of spin flip proposals thereby expanding the simulation time to collect reliable data. Unluckily, the system under consideration is such a system, but the following update algorithm could be the solution to this dilemma.

Line spin update algorithm

In this update method the microstate transition will be enabled both through a line flip and a single spin flip. A line flip consists of flipping all the spins highlighted gray in Figure 3.1. Of course, choosing other rows and columns is possible as well. The additional single spin flip is necessary to satisfy Condi-

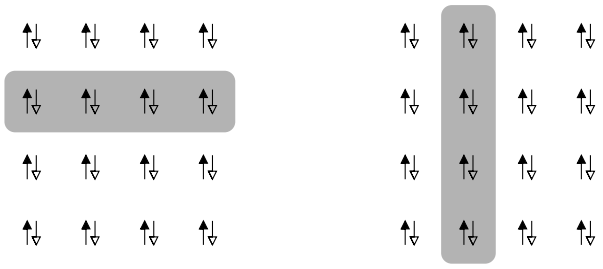

Figure 3.1: This Figure shows two line flip proposal of the $2L$ possible ones.

tion (18) because by only applying line flips, the entire state space cannot be covered. For example, the system is initiated in a nearly ideal ferromagnetic state, with one spin aligned in the opposite direction. There exists no sequence of line flips that transits the system from the initial state mentioned to an ideal ferromagnetic state, hence the system is trapped in a sub-state space. To apply this update method in practice, firstly choose a line at random of the $2L$ columns and rows with a selection probability $f_{ij} = 1/2L$. This line will be flipped with a probability $w_{ij} = \min\{1, \exp(-\Delta E/kT)\}$, but now ΔE results from a flipped line. After the line flip proposal one has to perform L spin flip proposals such that $L/2$ repetitions of this procedure correspond to one sweep. With this unit of simulation steps, the two depicted update algorithms are comparable.

The advantage of the modified algorithm is to overcome the high rejection rate in the frustrating temperature range of the system. The line flips mentioned in Section 2.1 applied to an aligned ground-state cost no energy, therefore the line flips are accepted more frequently at low T because the system is in a near ground-state and a line flip has low energy costs. This line spin update algorithm was first presented in a paper of Kalz et al. [1]

3.2 Pseudo random number generators

In the two previous subsection, the simulation algorithms depicted rely on stochastic experiments, in particular on the randomly chosen lattice sites or lines and the acceptance of the flip proposals. Even for the smallest considered lattice length, the number of such stochastic experiments amounts to many millions. Rolling the dice is definitely not the way to go, performing these stochastic experiments in a reasonable time. In computer simulation studies, pseudo random number generators (PRNG) overcome this problem. PRNG are based on

some deterministic rule, producing a sequence of numbers X_i with a random face, i.e., X_i appear to be drawn randomly. An example of such a deterministic rule is the linear congruential generators defined by the recursive sequence

$$X_{i+1} = (aX_i + c)\mathrm{mod}(m),$$

producing pseudo random numbers between 0 and $m-1$, with $a, c, m \in \mathbb{N}$ [22]. There are many of such algorithms, with advantages and disadvantages for their purposes. The main criterions are the period length, i.e., the number of iteration until the same sequence returns, and the efficiency in context of the computational workload. Furthermore, some algorithms exhibit a "resonant" behavior with some application, i.e., the randomness fails, and unreliable data can be produced [22]. Therefore, care is necessary for the choice of the PRNG.

For the numerical work in this thesis, the 32bit Mersenne Twister `mt19937` PRNG of the `c++11` standard library is used, which is considered as very well tested and as a common choice for Monte Carlo simulation studies. Additionally, this PRNG has a very large period length of $2^{19937}-1$.

Many of the PRNG and particularly the Mersenne Twister generator produces uniformly distributed integers. An additional step is necessary to obtain non-uniform distributed pseudo random number. For explanation, let be $P(x)$ some invertible probability distribution of the random variable X and $p \in [0, 1)$ a pseudo random number drawn uniformly. Thus, the probability of the event $X = x^*$ is given by $P(x^*)$. Then, a pseudo random number distributed according to $P(x)$ can be obtained through the inversion $x^* = P^{-1}(p)$. [22]

3.3 Error estimation

The idea of the simulation method described in Section 3.1 is to approximate the theoretical expectation value $\langle \mathcal{O} \rangle$ of a microstate dependent observable $\mathcal{O}(\boldsymbol{\sigma})$ through Equation (14). This estimate depends on the number of measurements M and the explicit outcomes of the stochastic experiments, and hence the estimator $\hat{\mathcal{O}}$ carries an error and fluctuates around the exact expectation value. One has to chose M properly such that the expense of simulation time and the statistical error of the estimate are in balance. A quantity to evaluate the deviation between $\hat{\mathcal{O}}$ and $\langle \mathcal{O} \rangle$ is the variance

$$\sigma^2_{\hat{\mathcal{O}}} = \langle \hat{\mathcal{O}}^2 \rangle - \langle \hat{\mathcal{O}} \rangle^2.$$

In the following, the term "error" refers to the square root of the variance also known as one-sigma-error. If all requirements of the Central Limit Theorem [23, p.246] are sufficiently fulfilled, roughly 68% of the independently estimated values will satisfy $\hat{\mathcal{O}} \in [\langle \hat{\mathcal{O}} \rangle - \sigma_{\hat{\mathcal{O}}}, \langle \hat{\mathcal{O}} \rangle + \sigma_{\hat{\mathcal{O}}}]$. The expression of the variance can be

rewritten using Equation (14)

$$\sigma^2_{\hat{\mathcal{O}}} = \frac{1}{M^2}\sum_{k,l=1}^{M} \langle \mathcal{O}(\boldsymbol{\sigma}_k)\mathcal{O}(\boldsymbol{\sigma}_l)\rangle - \langle \mathcal{O}(\boldsymbol{\sigma}_k)\rangle\langle \mathcal{O}(\boldsymbol{\sigma}_l)\rangle$$
$$= \frac{1}{M^2}\sum_{k=1}^{M}\left(\langle \mathcal{O}(\boldsymbol{\sigma}_k)^2\rangle - \langle \mathcal{O}(\boldsymbol{\sigma}_k)\rangle^2\right) + \frac{1}{M^2}\sum_{k\neq l}^{M}\left(\langle \mathcal{O}(\boldsymbol{\sigma}_k)\mathcal{O}(\boldsymbol{\sigma}_l)\rangle - \langle \mathcal{O}(\boldsymbol{\sigma}_k)\rangle\langle \mathcal{O}(\boldsymbol{\sigma}_l)\rangle\right).$$

The off-diagonal sum leads to an important quantity, namely the autocorrelation function defined as

$$A_{\mathcal{O}}(k,l) = \frac{\langle \mathcal{O}(\boldsymbol{\sigma}_k)\mathcal{O}(\boldsymbol{\sigma}_l)\rangle - \langle \mathcal{O}(\boldsymbol{\sigma}_k)\rangle\langle \mathcal{O}(\boldsymbol{\sigma}_l)\rangle}{\langle \mathcal{O}(\boldsymbol{\sigma}_k)^2\rangle - \langle \mathcal{O}(\boldsymbol{\sigma}_k)\rangle^2}.$$

The autocorrelation function serves as a benchmark of how much the k^{th} measurement of the observable $\mathcal{O}$ is correlated to the l^{th}, 1 for maximally correlated and 0 for uncorrelated. If the underlying probability distribution of the measurements is in equilibrium, and thus the observables $\mathcal{O}(\boldsymbol{\sigma}_k)$ and $\mathcal{O}(\boldsymbol{\sigma}_l)$ are distributed according to the same probability distribution, translation invariance will hold for the measurement indices within expectation values, i.e., for our purposes

$$\langle \mathcal{O}(\boldsymbol{\sigma}_k)\mathcal{O}(\boldsymbol{\sigma}_{k+(l-k)})\rangle = \langle \mathcal{O}(\boldsymbol{\sigma}_{\tilde{k}})\mathcal{O}(\boldsymbol{\sigma}_{\tilde{k}+(l-k)})\rangle \quad \text{and} \quad \langle \mathcal{O}(\boldsymbol{\sigma}_k)\rangle = \langle \mathcal{O}(\boldsymbol{\sigma}_{\tilde{k}})\rangle \quad \forall \tilde{k}.$$

With this assumption the autocorrelation function is only a function of the measurement indices delay $l-k$ and obtaining the simplified expression of the variance

$$\sigma^2_{\hat{\mathcal{O}}} = \frac{\sigma^2_{\mathcal{O}}}{M} + \frac{2}{M^2}\sum_{k=1}^{M}\sum_{l=k+1}^{M} \langle \mathcal{O}(\boldsymbol{\sigma}_k)\mathcal{O}(\boldsymbol{\sigma}_{k+(l-k)})\rangle - \langle \mathcal{O}(\boldsymbol{\sigma}_k)\rangle\langle \mathcal{O}(\boldsymbol{\sigma}_{k+(l-k)})\rangle$$
$$= \frac{\sigma^2_{\mathcal{O}}}{M} + \frac{2\sigma^2_{\mathcal{O}}}{M^2}\sum_{k=1}^{M}\sum_{l=k+1}^{M} A_{\mathcal{O}}(l-k) = \frac{\sigma^2_{\mathcal{O}}}{M} + \frac{2\sigma^2_{\mathcal{O}}}{M^2}\sum_{l-k=1}^{M}(M-(l-k))\cdot A_{\mathcal{O}}(l-k)$$
$$= \frac{\sigma^2_{\mathcal{O}}}{M}\left(1 + 2\sum_{l-k=1}^{M} A_{\mathcal{O}}(l-k)\left(1 - \frac{l-k}{M}\right)\right),$$

with $\sigma^2_{\mathcal{O}} = \langle \mathcal{O}(\boldsymbol{\sigma}_k)^2\rangle - \langle \mathcal{O}(\boldsymbol{\sigma}_k)\rangle^2$, which is independent of the index k. To resolve the double sum to a simple sum, one has to apply the factor $M-(l-k)$ because for a fixed delay $l-k$, the corresponding value of the autocorrelation function appears $M-(l-k)$ times in the double sum. This leads to the important quantity of integrated autocorrelation time

$$\tau_{\mathcal{O},\text{int}} = \frac{1}{2} + \sum_{l-k=1}^{M} A_{\mathcal{O}}(l-k)\left(1 - \frac{l-k}{M}\right). \tag{19}$$

The interpretation of the integrated autocorrelation time can best be explained by the expression of $\sigma^2_{\hat{\mathcal{O}}}$ above, rewritten in terms of the autocorrelation time $\sigma^2_{\hat{\mathcal{O}}} = 2\tau_{\mathcal{O},\mathrm{int}}\sigma^2_{\mathcal{O}}/M$ in comparison to the uncorrelated case $\sigma^2_{\hat{\mathcal{O}}} = \sigma^2_{\mathcal{O}}/M$ provided by the Central Limit Theorem [23, p.246]. Therefore, the number of uncorrelated measurements is M for uncorrelated data and $M/2\tau_{\mathcal{O},\mathrm{int}}$ for correlated data, implying only every $(2\tau_{\mathcal{O},\mathrm{int}})^{\mathrm{th}}$ measurement is uncorrelated. The data produced by MCMC methods is correlated, and hence one has to deal with autocorrelation times to estimate reliable statistical errors. [9]

The introduced autocorrelation function $A_{\mathcal{O}}(k,l)$ has a significant behavior for large delays $l-k$, which can be obtained by the proportional relation

$$\frac{\langle \mathcal{O}(\boldsymbol{\sigma}_k)\mathcal{O}(\boldsymbol{\sigma}_l)\rangle - \langle \mathcal{O}(\boldsymbol{\sigma}_k)\rangle\langle \mathcal{O}(\boldsymbol{\sigma}_l)\rangle}{\langle \mathcal{O}(\boldsymbol{\sigma}_k)^2\rangle - \langle \mathcal{O}(\boldsymbol{\sigma}_k)\rangle^2} \propto \exp\left(-\frac{l-k}{\tau_{\mathcal{O},\mathrm{exp}}}\right), \tag{20}$$

defining the exponential autocorrelation time $\tau_{\mathcal{O},\mathrm{exp}}$. For a perfect exponential decay and a transition into the continuum, these autocorrelation times coincide because the expression of $\tau_{\mathcal{O},\mathrm{int}}$ corresponds to an approximation of the integral

$$\int_0^\infty A_{\mathcal{O}}(t)\mathrm{d}t = \int_0^\infty \exp\left(-\frac{t}{\tau_{\mathcal{O},\mathrm{exp}}}\right)\mathrm{d}t = \tau_{\mathcal{O},\mathrm{exp}}.$$

Propagation of errors

During an analysis, one is interested in quantities f depending on some observables $\mathcal{O}^{(i)}$ for $i \in \{1,...,K\}$. Additionally, the estimates $\hat{\mathcal{O}}^{(i)}$ and corresponding variances σ_i^2 are already known. The variance σ_f^2 can then be obtained through a propagation of the variances σ_i^2. Firstly let's consider the linear terms of the Taylor-expansion of f at $(\hat{\mathcal{O}}^{(1)},...,\hat{\mathcal{O}}^{(K)})$

$$f(\mathcal{O}^{(1)},...,\mathcal{O}^{(K)}) - f(\hat{\mathcal{O}}^{(1)},...,\hat{\mathcal{O}}^{(K)}) \approx \sum_{i=1}^{K} \partial_i f \left(\mathcal{O}^{(i)} - \hat{\mathcal{O}}^{(i)}\right),$$

where $\partial_i f$ denotes the partial derivative with respect to $\mathcal{O}^{(i)}$ at $\hat{\mathcal{O}}^{(i)}$. But this approximation holds only for deviation $\mathcal{O}^{(i)}$–$\hat{\mathcal{O}}^{(i)}$ sufficiently small. To close the connection between these deviations and the variances σ_i^2, consider the infinite

statistics limit

$$\begin{aligned}\sigma_f^2 &= \lim_{M\to\infty}\left(\frac{1}{M}\sum_{j=1}^{M}\left(f(\mathcal{O}^{(1)}(\boldsymbol{\sigma}_j),...,\mathcal{O}^{(K)}(\boldsymbol{\sigma}_j)) - f(\hat{\mathcal{O}}^{(1)},...,\hat{\mathcal{O}}^{(K)})\right)^2\right)\\ &= \lim_{M\to\infty}\left(\frac{1}{M}\sum_{j=1}^{M}\left(\sum_{i=1}^{K}\partial_i f\left(\mathcal{O}^{(i)}(\boldsymbol{\sigma}_j)-\hat{\mathcal{O}}^{(i)}\right)\right)^2\right)\\ &= \sum_{i=1}^{K}(\partial_i f)^2 \lim_{M\to\infty}\left(\frac{1}{M}\sum_{j=1}^{M}\left(\mathcal{O}^{(i)}(\boldsymbol{\sigma}_j)-\hat{\mathcal{O}}^{(i)}\right)^2\right)\\ &\quad + \sum_{i\neq k}^{K}\partial_i f\partial_k f \lim_{M\to\infty}\left(\frac{1}{M}\sum_{j=1}^{M}\left(\mathcal{O}^{(i)}(\boldsymbol{\sigma}_j)-\hat{\mathcal{O}}^{(i)}\right)\left(\mathcal{O}^{(k)}(\boldsymbol{\sigma}_j)-\hat{\mathcal{O}}^{(k)}\right)\right).\end{aligned}$$

Using the infinite statistics limit in the opposite direction one gets the famous error-propagation formula

$$\sqrt{\sigma_f^2} = \left(\sum_{i=1}^{K}(\partial_i f)^2\sigma_i^2 + \sum_{i\neq k}^{K}\partial_i f\partial_k f\sigma_{ik}^2\right)^{1/2}, \tag{21}$$

with $\sigma_{ik}^2 = \lim_{M\to\infty}(\frac{1}{M}\sum_{j=1}^{M}(\mathcal{O}^{(i)}(\boldsymbol{\sigma}_j)-\hat{\mathcal{O}}^{(i)})(\mathcal{O}^{(k)}(\boldsymbol{\sigma}_j)-\hat{\mathcal{O}}^{(k)}))$ denoted as covariance. The usage of this formula demands errors small enough of the estimated means $\hat{\mathcal{O}}^{(i)}$. The off-diagonal sum can be omitted for uncorrelated observables $\mathcal{O}^{(i)}$, but this is not always the case. [24, p.39]

Jackknife analysis

In general, it is cumbersome to determine the autocorrelation function and the corresponding autocorrelation time or to obtain proper error estimations of observables resulting from non-linear functions of the measured observables through error propagation. A powerful tool to overcome these problems is Jackknife analysis. For explanation, let $\mathcal{O}(\boldsymbol{\sigma}_k)$ for $k \in \{1,...,M\}$ be the received measurements. Dividing this series into M_J blocks of length m_J such that $M = m_J \cdot M_J$ applies, then the j^{th} Jackknife block for $j \in \{1,...,M_J\}$ and its mean are defined by

$$\left\{\mathcal{O}(\boldsymbol{\sigma}_1),\mathcal{O}(\boldsymbol{\sigma}_2),...,\mathcal{O}(\boldsymbol{\sigma}_M)\right\} \setminus \left\{\mathcal{O}(\boldsymbol{\sigma}_{m_J(j-1)+1}),\mathcal{O}(\boldsymbol{\sigma}_{m_J(j-1)+2}),...,\mathcal{O}(\boldsymbol{\sigma}_{m_J j})\right\},$$

$$\mathcal{O}_j^J = \frac{1}{M-m_J}\left(\sum_{k=1}^{M}\mathcal{O}(\boldsymbol{\sigma}_k) - \sum_{k=1}^{m_J}\mathcal{O}(\boldsymbol{\sigma}_{m_J(j-1)+k})\right).$$

The mean value of the Jackknife blocks should coincide with the mean value of the original series of the measurements as the following calculation shows.

$$\hat{\mathcal{O}}^J = \frac{1}{M_J}\sum_{j=1}^{M_J}\mathcal{O}_j^J = \frac{1}{M_J(M-m_J)}\left(M_J\sum_{k=1}^{M}\mathcal{O}(\boldsymbol{\sigma}_k) - \sum_{j=1}^{M_J}\sum_{k=1}^{m_J}\mathcal{O}(\boldsymbol{\sigma}_{m_J(j-1)+k})\right)$$
$$= \frac{1}{m_J M_J(M_J-1)}(M_J-1)\sum_{k=1}^{M}\mathcal{O}(\boldsymbol{\sigma}_k) = \frac{1}{M}\sum_{k=1}^{M}\mathcal{O}(\boldsymbol{\sigma}_k) = \hat{\mathcal{O}}$$

The variance of the estimator $\hat{\mathcal{O}}$ can be computed by

$$\sigma^2_{\hat{\mathcal{O}}} = \frac{M_J-1}{M_J}\sum_{j=1}^{M_J}\left(\mathcal{O}_j^J - \hat{\mathcal{O}}\right)^2 \tag{22}$$

To see the validity of Equation (22), perform the following calculation

$$\frac{M_J}{M_J-1}\sigma^2_{\hat{\mathcal{O}}} = \sum_{j=1}^{M_J}\left(\frac{M}{M-m_J}\hat{\mathcal{O}} - \frac{m_J}{M-m_J}\hat{\mathcal{O}}_j^{\text{Block}} - \hat{\mathcal{O}}\right)^2$$
$$= \frac{m_J^2}{(M-m_J)^2}\sum_{j=1}^{M_J}\left(\hat{\mathcal{O}}_j^{\text{Block}} - \hat{\mathcal{O}}\right)^2 = \frac{1}{(M_J-1)^2}\sum_{j=1}^{M_J}\left(\hat{\mathcal{O}}_j^{\text{Block}} - \hat{\mathcal{O}}\right)^2,$$

where $\hat{\mathcal{O}}_j^{\text{Block}} = \frac{1}{m_J}\sum_{k=1}^{m_J}\mathcal{O}(\boldsymbol{\sigma}_{m_J(j-1)+k})$ were introduced for simplicity. Multiplying the above equation with M_J-1, one obtains on the right-hand side the unbiased variance estimator of the block means σ^2_{Block}. Furthermore, this results in the equation $\sigma^2_{\hat{\mathcal{O}}} = \sigma^2_{\text{Block}}/M_J$, which becomes true if the requirements of the Central Limit Theorem [23, p.246] are satisfied. The requirement of independently and identically distributed random variables demands uncorrelated $\hat{\mathcal{O}}_j^{\text{Block}}$, therefore one has to choose $m_J \gg \tau_{\mathcal{O}}$ such that Equation (22) turns valid. [9]

3.4 Least square approximation

Least square approximation is a tool useful for data analysis. To give an explanation, let (x_i, y_i) for $i \in \{1, ..., M\}$ be a set of data points where the values y_i have a variance σ_i^2, which should be fitted to a model $f_m(x)$ with m parameters yet to be determined. The idea is to maximize the probability W_m such that a given model f_m produces the data points (x_i, y_i). Under the Gaussian assumption, this probability is given by

$$W_m = \prod_{i=1}^{M}\left(\frac{1}{\sqrt{2\pi\sigma_i^2}}\right)\cdot\exp\left(-\frac{1}{2}\sum_{i=1}^{M}\frac{(y_i - f_m(x_i))^2}{\sigma_i^2}\right),$$

where the weighted sum in the exponent is also known as χ^2. Therefore, the m parameters must be chosen such that the value of χ^2 is minimal. For linear

models the minimum in the parameter space can be determined analytically but for non-linear models there are only methods for approximating the parameters minimizing χ^2. Another important quantity is the statistical degree of freedom dof of the estimated value of χ^2, which equals the difference of the number of random variables M and the number of determined means m, i.e., dof $= M-m$. [24, p.103]

The determined model parameters are obviously correlated. Thus, some attention is necessary for the error estimation of observables resulting from these parameters. Using the error-propagation Formula (21), the off-diagonal sum has be taken into account to receive a reliable error estimation.

Quality of the Least square approximation

The above consideration does not deliver an answer to which model represents the observed data better. To answer this question, let's consider the variance of the fit

$$\sigma^2_{\text{fit}} = \frac{1}{M-m}\sum_{i=1}^{M}\frac{1/\sigma_i^2}{1/M\sum_{i=1}^{M}1/\sigma_i^2}\cdot(y_i - f_m(x_i))^2$$

where the first factor in the sum weights the deviation of the data point to the model corresponding to the variance of the data point. This weighting factor can be rewritten as

$$\frac{1}{\sigma_i^2}\frac{1/M\cdot M}{1/M\sum_{i=1}^{M}1/\sigma_i^2} = \frac{1}{\sigma_i^2}\frac{1}{M}\sum_{i=1}^{M}\frac{1/\sigma_i^2}{1/M\sum_{i=1}^{M}1/\sigma_i^2}\cdot\sigma_i^2 = \frac{\hat{\sigma}^2}{\sigma_i^2}$$

where $\hat{\sigma}^2$ denotes the weighted average of the variance of the data points. Inserting the above identity into the variance of the fit gives the following expression of χ^2-value

$$\chi^2 = \text{dof}\frac{\sigma^2_{\text{fit}}}{\hat{\sigma}^2}.$$

For this equation one can discuss three extremal cases. Firstly, $\chi^2 \ll \text{dof}$, then $\sigma^2_{\text{fit}} \ll \hat{\sigma}^2$ implying that model parameters can always be found such that the model fits with the data points. This is also known as "overfitting". Secondly, $\chi^2 \gg \text{dof}$, thus $\sigma^2_{\text{fit}} \gg \hat{\sigma}^2$, i.e., the model does not fit with the observed data points and the third one, $\chi^2 \approx \text{dof}$, implies that the variance of the fit and the data points are roughly the same. Therefore, a χ^2-value of statistical degree of freedom should be the aim. [24, p.194]

3.5 Multi-histogram reweighing

Multi-histogram reweighing or weighted histogram analysis method (WHAM) is a powerful technique to obtain an observable as a function of the temperature

T as smooth curve. The multi-histogram reweighing refers to multiple temperatures in contrast to the simple histogram reweighing, referring to a single T. For explanation, let (T_i, M_i) for $i \in \{1, ..., m\}$ be the simulation points, i.e., the system was simulated at the temperature T_i with M_i measurements. The idea is to estimate the unknown density of states $\Omega(E)$ using the measurement of the observable

$$H_i(E) = \sum_{k=1}^{M_i} \delta_{EE_k},$$

also known as the unnormalized histogram. The index i denotes the simulation point at the temperature T_i, the index k refers to the k^{th} measurement of the energy at T_i and $\delta_{EE'}$ is the Kronecker-delta. This observable gives an estimator of the energy probability distribution

$$P_{T_i}(E) = \frac{\Omega(E)\exp(-E/kT_i)}{Z_{T_i}} \quad \text{therefore,} \quad \hat{P}_i(E) = \frac{H_i(E)}{M_i} \quad \text{holds.}$$

Implying an estimator for the density of states for each simulation point

$$\hat{\Omega}_i(E) = Z_i \exp(E/kT_i)\hat{P}_i(E) = Z_i \exp(E/kT_i)\frac{H_i(E)}{M_i},$$

the index i does only refer to the estimates at the corresponding simulation point, though the exact density of states is independent of T. Hence, these estimates has to be combined to a common one. This combination can be performed similarly to the weighed average of the differences between data points and the chosen model of the least square approximation, Section 3.4. Thus, the variance weighed average of the density of states should be computed by

$$\hat{\Omega}(E) = \sum_{i=1}^{m} \frac{1/\sigma^2_{\hat{\Omega}_i}(E)}{\sum_{i=1}^{m} 1/\sigma^2_{\hat{\Omega}_i}(E)} \hat{\Omega}_i(E),$$

with $\sigma^2_{\hat{\Omega}_i}(E)$ being the variance of $\hat{\Omega}_i(E)$ at an explicit energy E. Determining these variances by the following calculation

$$\begin{aligned}
\sigma^2_{\hat{\Omega}_i}(E) &= \frac{Z_i^2 \exp(2E/kT_i)}{M_i^2} \sigma^2_{H_i}(E) = \frac{Z_i^2 \exp(2E/kT_i)}{M_i^2} \left(\langle H_i(E)^2 \rangle - \langle H_i(E) \rangle^2 \right) \\
&= \frac{Z_i^2 \exp(2E/kT_i)}{M_i^2} \left(\sum_{k,l=1}^{M_i} \langle \delta_{EE_k} \delta_{EE_l} \rangle - \sum_{k,l=1}^{M_i} \langle \delta_{EE_k} \rangle \langle \delta_{EE_l} \rangle \right) \\
&= \frac{Z_i^2 \exp(2E/kT_i)}{M_i^2} \left(\sum_{k=1}^{M_i} \langle \delta^2_{EE_k} \rangle - \langle \delta_{EE_k} \rangle^2 + \sum_{k \neq l}^{M_i} \langle \delta_{EE_k} \delta_{EE_l} \rangle - \langle \delta_{EE_k} \rangle \langle \delta_{EE_l} \rangle \right),
\end{aligned}$$

the expressions in the brackets can be rewritten in terms of quantities mentioned in Section 3.3. [9]

To do that let's consider the first term, which is the variance of the observable δ_{EE_k}. It holds that $P_{T_i}(E) = \langle H_i(E)\rangle / M_i$ because $H_i(E)/M_i$ is an estimator of $P_{T_i}(E)$ and the expectation value of an estimator should be coincided with the theoretical one. Assuming an equilibrated distribution of the measurement δ_{EE_k}, then it should always also hold that $\langle \delta_{EE_k}\rangle = \langle \delta_{EE_l}\rangle$ for all k, l. Hence, the expectation value of $H_i(E)$ can be expressed as

$$M_i P_{T_i}(E) = \langle H_i(E)\rangle = \left\langle \sum_{k=1}^{M_i} \delta_{EE_k} \right\rangle = \sum_{k=1}^{M_i} \langle \delta_{EE_k}\rangle = M_i \langle \delta_{EE_{\tilde{k}}}\rangle_i \quad \forall \tilde{k},$$

and thus $P_{T_i}(E) = \langle \delta_{EE_{\tilde{k}}}\rangle_i$ holds for all $\tilde{k}$. Therefore, it follows for the variance of δ_{EE_k} that

$$\sigma^2_{\delta,i}(E) = \sum_{k=1}^{M_i} \langle \delta^2_{EE_k}\rangle - \langle \delta_{EE_k}\rangle^2 = \sum_{k=1}^{M_i} \langle \delta_{EE_k}\rangle - \langle \delta_{EE_k}\rangle^2 = M_i P_{T_i}(E)(1 - P_{T_i}(E)).$$

The second expression in the brackets describes the correlation between the measurements. Resolving this one in terms of the integrated autocorrelation time of Equation (19) with $\mathcal{O}(\boldsymbol{\sigma}_k) = \delta_{EE_k}$ leads to

$$\sum_{k\neq l}^{M_i} \langle \delta_{EE_k}\delta_{EE_l}\rangle - \langle \delta_{EE_k}\rangle\langle \delta_{EE_l}\rangle = 2\sigma^2_{\delta,i}(E)\left(\tau_{\mathrm{int},i}(E) - \frac{1}{2}\right).$$

These rewritten terms are inserted in the variance of $\hat{\Omega}_i(E)$ and further it is assumed that the simulated system has a large number of possible energies E such that $P_{T_i}(E)$ is much smaller than one, resulting in

$$\begin{aligned}
\sigma^2_{\hat{\Omega}_i}(E) &= \frac{Z_i^2 \exp(2E/kT_i)}{M_i^2} \sigma^2_{\delta,i}(E)\left(1 + 2\left(\tau_{\mathrm{int},i}(E) - \frac{1}{2}\right)\right) \\
&= \frac{Z_i^2 \exp(2E/kT_i)}{M_i/(2\tau_{\mathrm{int},i}(E))} P_{T_i}(E)(1 - P_{T_i}(E)) = \frac{Z_i^2 \exp(2E/kT_i)}{M_i/(2\tau_{\mathrm{int},i}(E))} P_{T_i}(E) \\
&= \frac{Z_i \exp(E/kT_i)}{M_i/(2\tau_{\mathrm{int},i}(E))} \Omega(E).
\end{aligned}$$

In the penultimate step, $(1 - P_{T_i}(E))$ is set to unity, because the above assumption is satisfied by the system under consideration for the corresponding lattice lengths. Using this term for the variance weighed average of the density of states

$\hat{\Omega}(E)$ leads to

$$\begin{aligned}\hat{\Omega}(E) &= \frac{\sum_{i=1}^{m} \frac{M_i}{2\tau_{\mathrm{int},i}(E)} Z_i^{-1} \exp(-E/kT_i)\hat{\Omega}_i(E)/\Omega(E)}{\sum_{i=1}^{m} \frac{M_i}{2\tau_{\mathrm{int},i}(E)} Z_i^{-1} \exp(-E/kT_i)/\Omega(E)} \\ &= \frac{\sum_{i=1}^{m} \frac{M_i}{2\tau_{\mathrm{int},i}(E)} \hat{P}_i(E)}{\sum_{i=1}^{m} \frac{M_i}{2\tau_{\mathrm{int},i}(E)} Z_i^{-1} \exp(-E/kT_i)} \\ &= \frac{\sum_{i=1}^{m} H_i(E)/(2\tau_{\mathrm{int},i}(E))}{\sum_{i=1}^{m} \frac{M_i}{2\tau_{\mathrm{int},i}(E)} Z_i^{-1} \exp(-E/kT_i)},\end{aligned}$$

where it should be emphasized, that $\Omega(E)$ is the exact density of states and therefore independent of the index i, and hence $\Omega(E)$ cancels out. In a practical context, the estimator above is not useable in a conventional way because the values of the partition function Z_i at the corresponding T_i are unknown. This dilemma can be solved by choosing a set of arbitrary Z_i inserting these into $\hat{\Omega}(E)$ and computing

$$Z_j = \sum_E \frac{\sum_{i=1}^{m} H_i(E)/(2\tau_{\mathrm{int},i}(E))}{\sum_{i=1}^{m} \frac{M_i}{2\tau_{\mathrm{int},i}(E)} Z_i^{-1} \exp(-E/kT_i)} \exp(-E/kT_j) \quad \text{for} \quad j \in \{1, ..., m\}.$$

Finally, this procedure has to be repeated with the new values of Z_i until the required accuracy is achieved. This delivers a converging algorithm to estimate the density of states. [9]

Usually, two main problems appear in practice. Firstly, computing $\tau_{\mathrm{int},i}(E)$ for each simulation point and all corresponding energy bins is quite cumbersome. In most works, these autocorrelation times are neglected e.g. [25], which is also done in the implementations of this thesis. Secondly, evaluating the sums in the nominator and denominator of $\hat{\Omega}(E)$ mostly results in huge numbers. Working with the logarithm of the nominator and denominator avoids overflow errors in implementations. However, this leads to the question of how to perform the summation without overflows. For example, the evaluation of $\ln(s_k)$ where $s_k = \sum_{i=1}^{k} \exp(x_i)$ for $k \in \{1, .., m\}$ should be done without dealing directly with the huge numbers $\exp(x_i)$. The following identity can be used iteratively

$$\ln(s_{k+1}) = \begin{cases} x_{k+1} + \ln(1 + \exp(\ln(s_k) - x_{k+1})) & \text{for } \ln(s_k) \leq x_{k+1} \\ \ln(s_k) + \ln(1 + \exp(x_{k+1} - \ln(s_k))) & \text{for } \ln(s_k) > x_{k+1} \end{cases}.$$

4 Results

In this thesis, the Monte Carlo simulation data is obtained using MCMC methods depicted in Subsection 3.1. Particularly, the described single spin update and line spin update algorithms are used to simulate the system under consideration at different temperatures T. For the numerical work the units are chosen such that $J_1 = k = 1$. Further, T is measured in units of J_1/k. In this Chapter 4, the term $M_{(\cdot)}$ refers to the estimates of the observable $|\mathcal{M}_{(\cdot)}(\boldsymbol{\sigma})|$.

4.1 Equilibrium properties

For the data collection of the free energy derivatives, the line spin update algorithm is used only. The system is simulated for the lattice lengths $L \in \{30, 40, 50, ..., 120\}$ and the NNN-interaction constant $J_2 = -0.5$, where the simulation parameters are chosen according to the Tables A.1 and A.2. Additionally, some consistency checks are performed for $L \in \{50, 80, 100\}$ and $J_2 \in \{-0.3, -0.6\}$, Appendix A.2. The corresponding data is received through a single independent cooling run, i.e., a different PRNG seed is used for each temperature. Furthermore, the system is initiated in a uniformly distributed state and is cooled to the corresponding temperature within a sufficient number of equilibration sweeps.

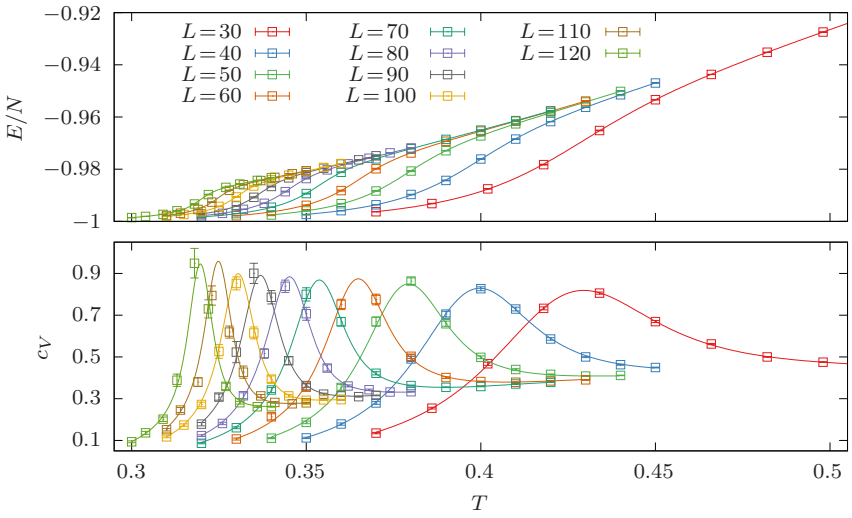

Figure 4.1: The plots show the energy per lattice site (top) and specific heat (bottom) as function of the temperature for different lattice length. The squares refer to the means and errors and the lines to the WHAM data.

Then, the internal energy E, Equation (5), the conventional magnetization M, Equation (6), specific heat c_V, Equation (7) and susceptibility χ, Equation (8) are measured and shown in Figures 4.1 and 4.2. Additionally, the data of the magnetization and susceptibility in the super-antiferromagnetic case Equation (10) are depicted as well, Figure 4.2.

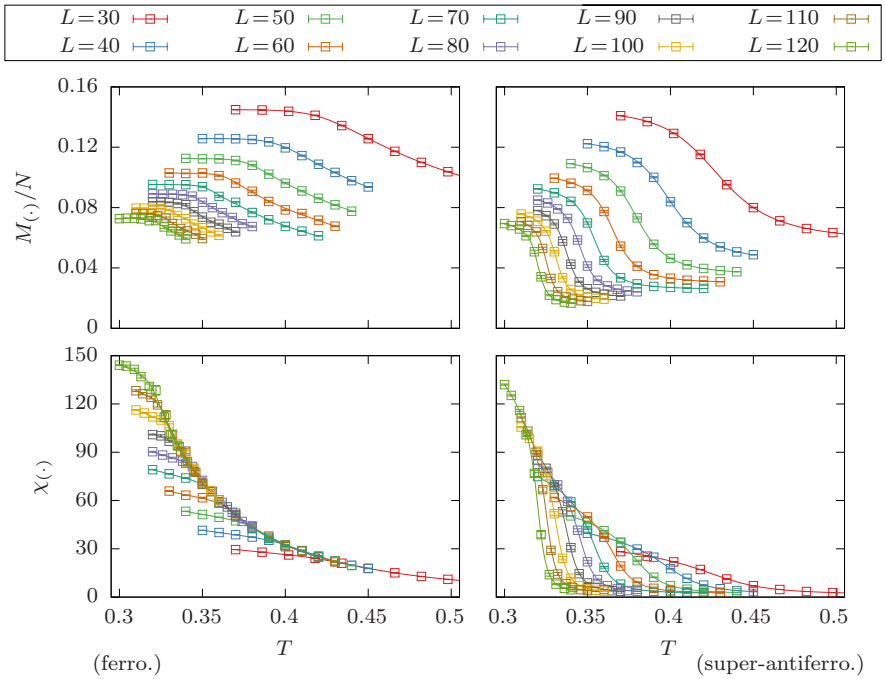

Figure 4.2: The magnetization per lattice site and susceptibility are shown in this figure, the left column refers to the ferromagnetic observables and the right column to the super-antiferromagnetic ones.

In the plots, all the means and errorbars are obtained by the Jackknife analysis described in Subsection 3.3. In addition, the density of states is estimated by WHAM, Section 3.5, and hence the smooth curves of E and c could easily be received. For the observables depending on the magnetization, the lists defined by Equation (3) are stored for each energy-bin in addition to the histograms. Thus, the resulting effective observables and the estimated density of states are combined to smooth curves of M, M_S and χ, χ_S.

Further, the peak locations of the specific heat data are analyzed more accurately. The numerical values of the maxima and their errors are shown in Table 4.1. They are obtained by measuring smaller histograms during the simulation run. Afterwards, the entire histogram of a simulation point is subtracted by these smaller histograms, resulting in a set of Jackknife histograms. These Jackknife histograms are combined to a set of densities of states estimated by

WHAM, succeeding in a set of specific heat curves and their peak locations $(T_{\max}, c_{V,\max})$. The mean of these maximums is determined by the conventional average and their error are computed taking the square root of Equation (22).

L	$T_{\max}$	$c_{V,\max}$	$T_{\max}$ in Ref. [1]	$T_{\max}$ in Ref. [2]
30	0.42946(24)	0.8187(27)	0.4289	0.4293
40	0.39969(27)	0.8289(53)	0.3988	0.3996
50	0.37933(31)	0.8497(88)	0.3798	0.3799
60	0.36492(38)	0.874(13)	0.3668	0.3653
70	0.35374(33)	0.869(16)	0.3536	0.3541
80	0.34522(27)	0.884(16)	0.3449	0.3447
90	0.33692(33)	0.891(19)	0.3356	0.3373
100	0.33054(25)	0.899(18)	0.3311	0.3307
110	0.32483(24)	0.958(22)	–	0.3256
120	0.31968(23)	0.945(28)	0.3188	0.3209

Table 4.1: This table depicts the specific heat peak locations corresponding to the lattice lengths and the reference data.

4.2 Dynamical properties

For the studies of the spin autocorrelation function $G(t_1, t_2)$, described by Equation (9) and their vertical and horizontal striped modifications, both the single spin update and the line spin update are employed. In the following, $t_1 = 0$ refers to the time of the beginning data collection, i.e., $\boldsymbol{\sigma}(t_1 = 0)$ corresponds to the state of the system after the equilibration period. In this fashion, t_2 refers to the time of the measurement in units of single spin sweeps, i.e., only the single spin flip proposals contributes to a sweep. The system is simulated for the lattice length $L \in \{32, 64, 128\}$ and the NNN-interaction constant $J_2 = -0.5$ by a dependent run in analogy to Ref. [3], i.e., the system is initialized in state referring to a low (or high) temperature, before it is slowly cooled (or warmed) to the nearest temperature and so on. A sufficient number of equilibration sweeps are performed between each temperature change, Figure 4.3. All of the data presented and in particular the errors are obtained by multiple dependent runs with different PRNG seeds. Hence, the thermodynamic expectation value of the measured autocorrelation function Equation (9) is substituted by the configurational expectation value. This replacement and method of error observation is motivated by the possibility that the system undergoes a glassy transition for $J_2 = -0.5$. Therefore, the equilibrium assumption of the probability distribution underlying the measurements may be violated as well as the time translation invariance of the autocorrelation function mentioned in Section 3.3. In other words $G(t_1, t_2)$ is not a function of the time delay $t_2 - t_1$ and the expectation value appearing in $G(t_1, t_2)$ cannot be estimated by a single run.

The dependent warming runs are performed with the ferromagnetic, horizon-

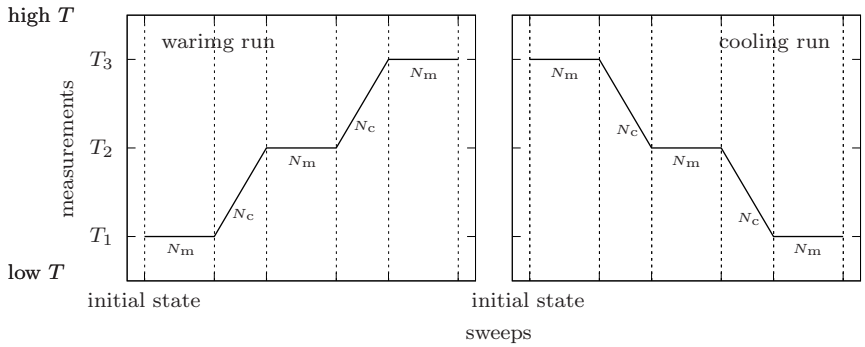

Figure 4.3: The figure depicts the scheme of data collection for the high T quench (warming run) and the low T quench (cooling run), where N_m denotes the sweeps for data collection of $G(t_1, t_2)$ and N_c denotes the number of equilibration sweeps.

tal and vertical striped initial states (Figure 4.3), the corresponding simulation parameters are chosen according to Table B.1. The values of the spin autocorrelation functions are measured for varying temperatures at $t_1 = 0$ and different t_2. The data shows no significant changes for different initial states, and thus only the case with the ferromagnetic initial state is shown in Figure 4.4. Additionally, the acceptance rate r_a of the single spin flip proposals and the line flip proposals are measured and shown in Figure 4.5.

For the dependent cooling run, the simulated system size is $L = 128$ with the depicted simulation parameters in Table B.1. The system under consideration is initiated in a high temperature state, corresponding to spin values distributed uniformly. Afterwards, it is cooled to the considered temperatures and the corresponding spin autocorrelation functions are measured analogously to the warming run (Figure 4.3). Their relaxation times τ are defined as the time the autocorrelation function falls below the numerical value 0.01 for a fixed temperature, in analogy to Timmons et al. [3]. The autocorrelation functions are approximated according to the exponential decay, Relation (20), using ranged least square approximations, Section 3.4, with the model $f(t_2) = A \exp(-t_2/\tau_\mathrm{exp})$. Then, only the range of $G(0, t_2)$ exponentially behaving contributes to the fits, obtained by half logarithmic plots. Rearranging the resulting model, which is set to 0.01 leads to

$$\tau = \tau_\mathrm{exp} \ln(100A)$$
$$\sigma_\tau^2 = \ln(100A)^2 \sigma_{\tau_\mathrm{exp}}^2 + \left(\frac{\tau_\mathrm{exp}}{A}\right)^2 \sigma_A^2 + \frac{\tau_\mathrm{exp} \ln(100A)}{A} (\sigma_{A,\tau_\mathrm{exp}}^2 + \sigma_{\tau_\mathrm{exp},A}^2),$$

with the model parameters A, τ_exp. The single indexed σ^2 denotes the variances and the double indexed ones the covariances. The variance of τ is obtained by the error propagation Formula (21). The received relaxation times are shown

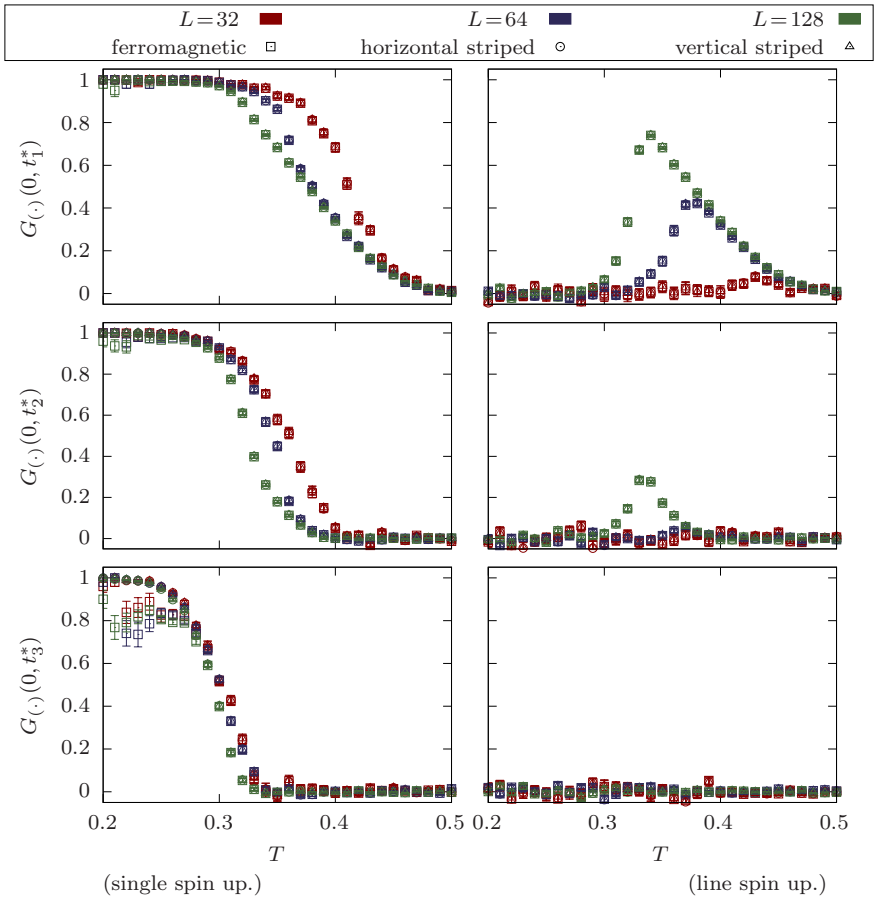

Figure 4.4: This plot shows the different variations of the spin autocorrelation functions at $t_1^* = 900$, $t_2^* = 9000$ and $t_3^* = 90000$ as a function of T for the corresponding update algorithms.

in Figure 4.6. The approach is intended by avoiding storing large amounts of autocorrelation function values until the value 0.01 is reached, which is nontrivial, especially for low temperatures. Usually, the number of necessary data is smaller for receiving reliable fits.

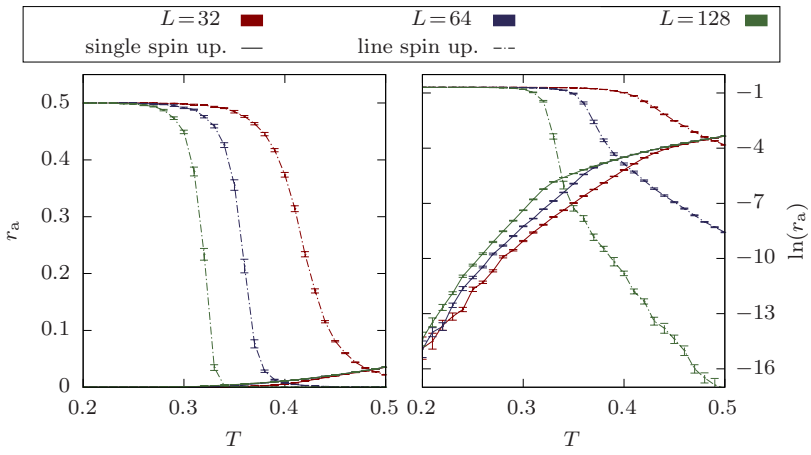

Figure 4.5: The acceptance rates are shown for the corresponding simulation algorithms and the lattice length.

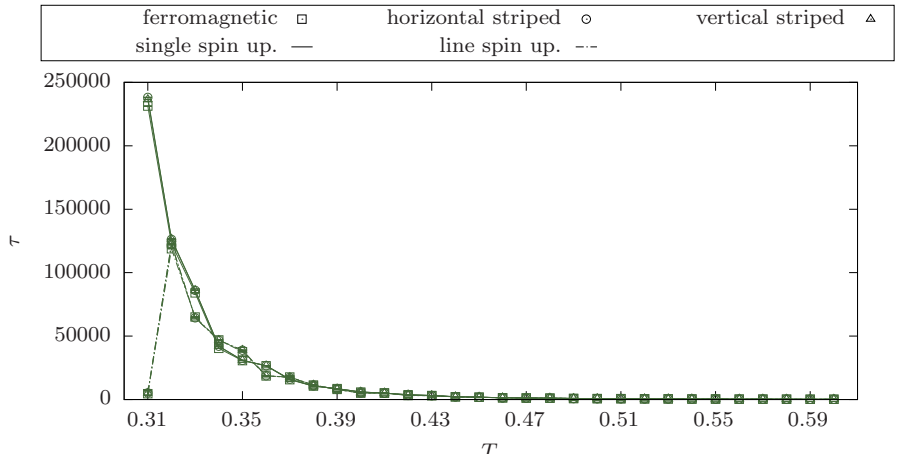

Figure 4.6: The relaxation times of the corresponding ordering premise as function of the temperature is shown for $L = 128$ and the used simulation algorithms.

4.3 Data interpretation

The procedure of data collection is separated from the interpretation, because the collected data is indisputable, but the interpretation is up for debate and does not deliver a final conclusion. In this Section 4.3, all simulation results of the previous two Sections are analyzed and connected to the physical properties depicted in Chapter 2, particularly to the statistical physics treatment and to the studies of critical phenomena, mentioned in Section 2.2 and 2.3.

Equilibrium properties

Considering the energy dependent observables in Figure 4.1, the behavior of the internal energy per lattice site as a function of T exhibits an inflection point with a positive slope. This implies a maximum of its first derivative, more precisely of the specific heat c_V according to the first equal sign in Equation (7). Generally, a maximum in the specific heat data for finite system sizes may indicate critical phenomena, which is not always the case, e.g., the one dimensional Ising model. Especially the narrowing and the slightly growing when increasing L suggests a divergence in the thermodynamic limit. The movement of the maximum locations proposes $T_{\max} = 0$ for $N \to \infty$, i.e., the system does not undergo a phase transition at a finite temperature. To confirm this presumption, the data in Table 4.1 is fitted to two different laws connecting the temperature near criticality with the spatial correlation length, i.e., the lattice length L for the finite systems under consideration.

The first law is originated by a paper of Kalz et al. [1], suggesting a power divergence of the spatial correlation length according to the continuous phase transitions with singularities in the second derivatives of the free energy. With Equation (11) under the assumption of $T_c = 0$ and the redefinition $\rho = -1/\nu$, the corresponding fit function results in

$$T_{\max}(L) = A \cdot L^{\rho},$$

where A denotes some proportional constant.

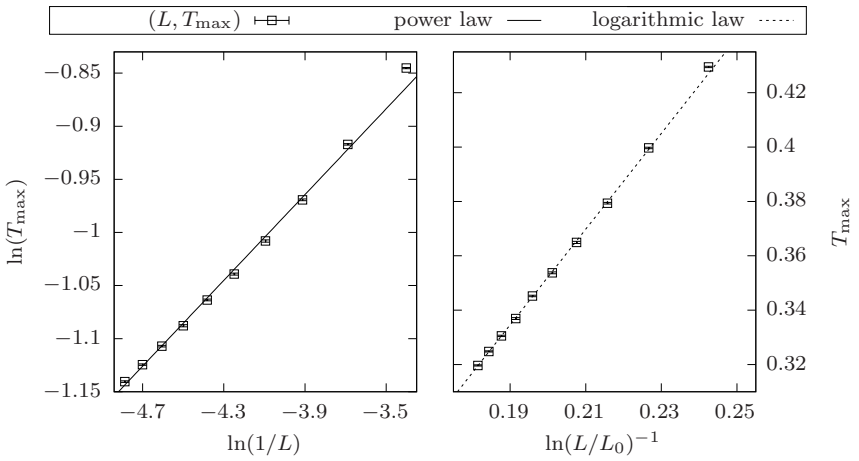

Figure 4.7: The mentioned fit approaches are plotted in this figure with rescaled axes such that the corresponding law behaves linear.

The second law is introduced by a work of Lee et al. [2], predicting an exponential divergence in the fashion of Equation (12). Landau et al. study the considered system for varying J_2/J_1 [13]. They conclude $\overline{\nu} \approx 1$ in an analysis

of the critical temperature as function of these ratios $T_c(J_2/J_1)$. With that and the assumption of $T_c = 0$, the second fit function becomes

$$T_{\max}(L) = A \cdot \ln(L/L_0)^{-1},$$

with some proportional constant A and the characteristic length scale L_0.

The corresponding fits are realized with the least square approximation described in Section 3.4. The best fits could be observed by taking finite size effects into account, i.e., the smallest lattice length $L = 30$ is neglected. They are shown in Figure 4.7, the associated model parameters and χ^2-values are depicted in Table 4.2.

The model of the exponential divergence shows a normalized χ^2-value close to the ideal value 1, suggesting a model representing the observed data. Further, the corresponding model parameters agree with the depicted one in Ref. [2], $L_{0,\text{Lee}} = e^{-0.736} = 0.479$.

The normalized χ^2-value of the power divergence approach is much larger than the ideal one, implying that the model does not represent the observed data. Unfortunately, its determined model parameters deviates from the presented ones in Ref. [1], $A_{\text{Kalz}} = 0.881(1)$ and $\rho_{\text{Kalz}} = -0.214(1)$, even taking all of the uncertainties into account. The best agreements to the presented ones in Ref. [1] could be observed by neglecting finite size effects[1].

power divergence

A	ρ	χ^2/dof
0.838(11)	−0.2020(31)	19.042

exponential divergence

A	L_0	χ^2/dof
1.7609(87)	0.485(12)	2.08

Table 4.2: The model parameters and χ^2-values of the least square approximations are shown for the corresponding divergence law.

The final consideration treats the magnetic observables for the ferromagnetic and super-antiferromagnetic cases in Figure 4.2. The associated magnetization per lattice site increase slightly when lowering temperature until a plateau is reached. Perhaps, this behavior results from coexisting domains of ferromagnetic and super-antiferromagnetic ordering similarities. Further, the numerical values of the plateaus decrease when increasing L.

This can be explained by the consideration of the observables $|\mathcal{M}_{(\cdot)}(\boldsymbol{\sigma})|$ as the square root of the random variable $Y_{(\cdot)}$ defined by

$$Y_{(\cdot)} = \sum_{i=1}^{N} \sigma_{(\cdot),i}^2,$$

[1] Taking $L = 30$ into account and accepting higher χ^2-values results in $A = 0.878(15)$, $\rho = -0.2123(40)$ and $\chi^2/\text{dof} = 68.137$ for the power divergence.

where $\sigma_{(\cdot),i}$ denotes the conventional or super-antiferromagnetic spin values. According to the Central Limit Theorem [23, p.246], it should $\langle Y_{(\cdot)}\rangle = N\langle\sigma^2_{(\cdot),i}\rangle$ holds with the expectation value $\langle\sigma^2_{(\cdot),i}\rangle$, being independent of N. Its square root can be estimated by $(\hat{Y}_i/N)^{1/2} = M_{(\cdot)}/\sqrt{N}$. Hence, the plateaus of the magnetization divided by $\sqrt{N}$ coincides at a numerical value, shown in Figure 4.8.

The corresponding susceptibilities as function of T show a declining exceed but no peak in the temperature range with significant behavior of E and c.

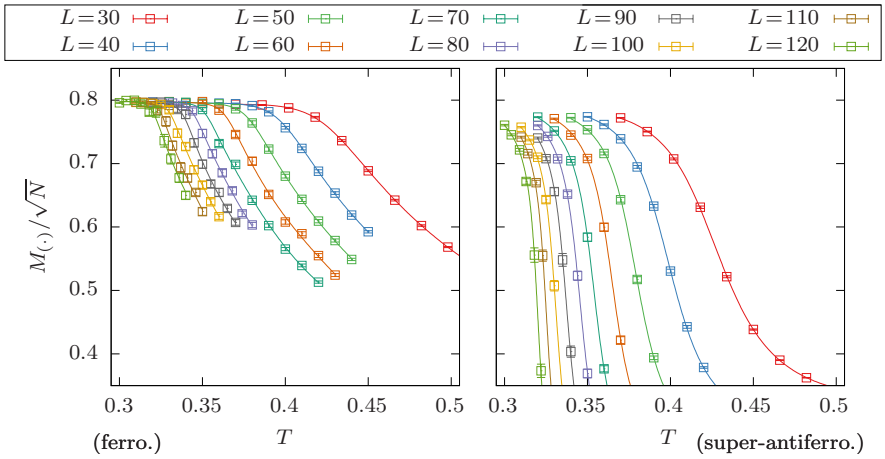

Figure 4.8: This figure depicts the presumed coinciding of the magnetization plateaus.

Dynamical properties

The measured spin autocorrelation function $G_{(\cdot)}(t_1, t_2)$, Equation (9), evaluates changes of similarities after a duration under the premise of ordering, i.e., $G_{(\cdot)}(t_1, t_2)$ becomes 1 if $\boldsymbol{\sigma}(t_1)$ and $\boldsymbol{\sigma}(t_2)$ appear equally similar or equally dissimilar under the corresponding premise and becomes less 1 if these states have changes in their similarities. The above ordering premise is associated to the ferromagnetic, horizontal and vertical striped patterns. In the following, the data of $G_{(\cdot)}(t_1, t_2)$, received by the non-equilibrium protocols described in Section 4.2, is interpreted for the warming run (high T quench) and cooling run (low T quench). During these examinations, the procedure is performed for single spin update, to check the consistency to the findings in Ref. [3]. Further, this routine is repeated for the line spin update, to conclude that the findings in Ref. [3] are perhaps indications of a glassy behavior or of a dynamic effects of the used simulation algorithm.

High temperature quench

In the following, the term "exceeding range" intends to the temperature range where $G_{(\cdot)}(t_1, t_2)$ increases effectively from 0.1 to 0.9 and the explanation refer to the spin autocorrelations $G_{(\cdot)}(0, t^*)$ of the single spin update in Figure 4.4 (left column). The exceeding range moves slowly to lower T when increasing the time t^* of the measurement.

For small t^* in the exceeding range, there are system size dependent differences of $G_{(\cdot)}(0, t^*)$ noticeable. A system with a smaller lattice length L appears more correlated for higher temperatures T, which may be originated by a smaller absolute number of spin flip proposals (sweeps $\propto L^2$) during a nearly unvarying acceptance rate, Figure 4.5.

This behavior should be fading for a higher statistics, and indeed it is the case for larger t^*. All of the $G_{(\cdot)}(0, t^*)$ remain in excess for low T at large t^*, originated by the frustration of the system.

Considering the plot of $G_{(\cdot)}(0, t^* = 90000)$ in Figure 4.4 (left column), the ferromagnetic spin autocorrelation drops slightly at lower T for the warming run with a ferromagnetic initialization. Therefore, the pattern at $t^* = 90000$ slightly deviates in average from the initial one, resulting in a small decline of $G_{(\cdot)}(0, t^*)$. In comparison, the $G_{(\cdot)}(0, t^* = 90000)$ of the other ordering premises (striped) remains at a value close to 1. Hence, the patterns of the microstates after 0 and 90000 sweeps appear equally dissimilar under the striped ordering premises, because for a decrease of the striped spin autocorrelations, the system has to spontaneously order (in average) in a striped state, being highly unlikely for systems with a high degeneracy $2^{L+1} - 1$, Section 2.1. Or simply put, it is more likely for the system to transits into one of the many dissimilar states, then into one of the few similar states. It should be emphasized that an analogous behavior could be observed for horizontal or vertical striped initialization.

Considering the spin autocorrelations of the line spin update in Figure 4.4 (right column), there are significant differences for small temperatures to the single spin update visible. For low T, all of the spin autocorrelations $G_{(\cdot)}(0, t^*)$ drop immediately to 0, because the line flip is accepted with a high probability, Figure 4.5, and they easily transit the system between the metastable states, Section 2.1. This drop is originated by the fact that a short sequence of line flips generates easily all the considered ordering patterns, Section 2.1. Hence, their application destroys the similarities under the considered ordering premises within a few sweeps, resulting in a decrease of $G_{(\cdot)}(0, t^*)$.

The spin autocorrelations are only nonvanishing for small t^*, showing peaks. The following explanation connects this behavior to the used update algorithm, referring to Figure 4.9.

For the transitions between high temperature states (high T), a smaller amount of line flips in the update (spin and line flips) sequence results in smaller free energy barriers. This fact and the relatively high acceptance rate of the spin flips reduces the numerical value of $G_{(\cdot)}(0, t^*)$.

When lowering the temperature, the frustration emerges markedly and in-

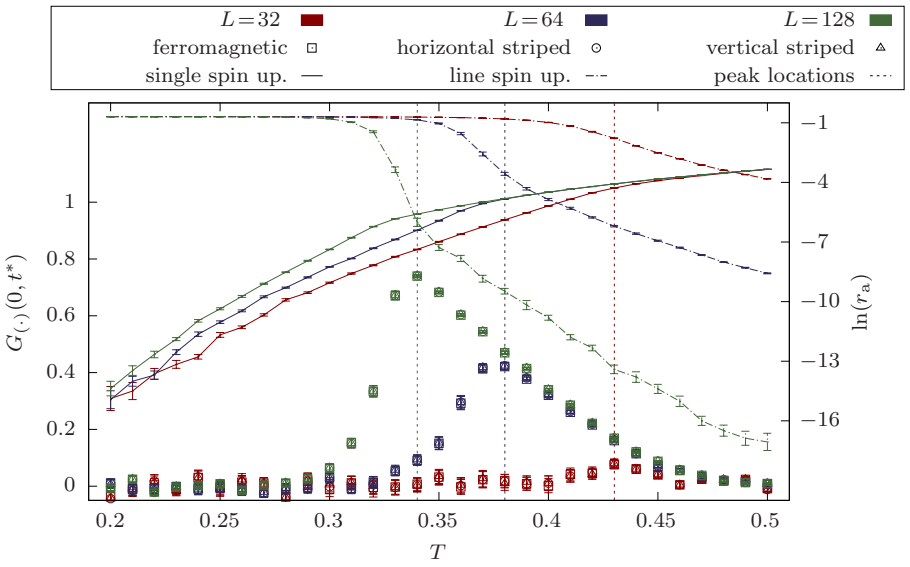

Figure 4.9: This plot combines the spin autocorrelations at $t^* = 900$ and acceptance rates as a function of the temperature for the warming run of the line spin update. The right vertical axis refers to the values of the spin correlations (squares) and the left one to the logarithm of the acceptance rates (lines).

creases the spin autocorrelations until the line flip acceptance rate exceeds the spin flip acceptance rate. A subsequent decline of $G_{(\cdot)}(0, t^*)$ to 0 is the result of the further growing line flip acceptance rate.

When increasing L, the peak enlarges and moves to lower T, caused by the movement of the intersection point of the corresponding acceptance rates. This movement is originated by lower energy costs of line flips for smaller L, effecting a higher acceptance probability with fixed T ($\propto \exp(-\Delta E/kT)$), Section 3.1. Thus, for small L the line flip acceptance exceeds the spin flip acceptance at higher T.

Another, finding is the slight increase of the $G_{(\cdot)}(0, t^*)$ errors, when the line flip update markedly emerges. It should be emphasized that all of the observations are independent of the initialization state and of the considered ordering premise.

Low temperature quench

Considering the obtained relaxation times for the dependent cooling run in Figure 4.6, the data of the single spin update shows a rapid increase when lowering T.

This suggests a divergence, and therefore an indication of a glassy behavior, Section 2.3. In analogy to Ref. [3], the nature of the divergence is assumed

according to a power law, leading to the fit function

$$\tau(T) = A|T - T_g|^{\rho}.$$

Performing the least square approximation with this model leads to an estimate of glass transition temperature T_g. The same data is fitted to the Vogel-Fulcher law (13) as well as in Ref. [3], implying the fit model

$$\tau(T) = A \exp(c/(T - T_K)).$$

This delivers a method to estimate the ideal glass transition temperature T_K, Section 2.3.

The corresponding fits and determined parameters are depicted in Figure 4.10 and Table 4.3. All of the obtained model parameters are slightly out of the tolerances in comparison to the values in Ref. [3], $T_g = 0.261(1)$, $\rho = 3.38(2)$ and $T_K = 0.091(5)$. Perhaps, this results from the low statistics of the used data, because the means and the errors are obtained by only four different runs[2]. The deviations of T_g may be caused by a differently chosen cooling rate then in Ref. [3].

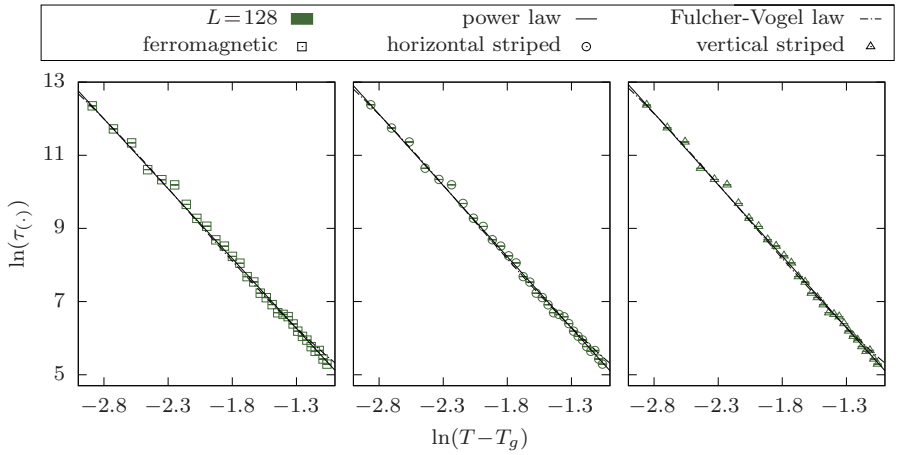

Figure 4.10: The full logarithmic plots show the corresponding relaxation times as function of a rescaled temperature and the determined fit models.

In comparison to τ of the single spin update, the relaxation times of the line spin update show no continuing increase rather an increase with a subsequent sharp decline, Figure 4.6. This behavior can be explained by considering Figure 4.11, depicting additionally the acceptance rates to the relaxation times.

It is noticeable that the relaxation times curves split when the line spin update acceptance exceeds the single spin update one by some magnitudes. Hence, the visible differences result from the emerging line spin update as well.

[2]The low statics is accepted to limit the corresponding computing time to 6 days.

power law

ordering premise	A	T_g	ρ
ferromagnetic	3.67(72)	0.2545(41)	3.82(15)
horizontal striped	3.36(61)	0.2530(39)	3.90(15)
vertical striped	3.32(60)	0.2526(39)	3.91(15)

Vogel-Fulcher law

ordering premise	A	T_K	c
ferromagnetic	4.1(1.5)	0.135(11)	1.91(18)
horizontal striped	3.6(1.3)	0.131(10)	1.98(17)
vertical striped	3.5(1.2)	0.131(10)	1.98(17)

Table 4.3: This table depicts the received parameters for the corresponding models.

However, the measured values of the line spin update relaxation times remain at large numerical values, $\tau = 4584(1358)$ at $T = 0.31$, but show no singular behavior.

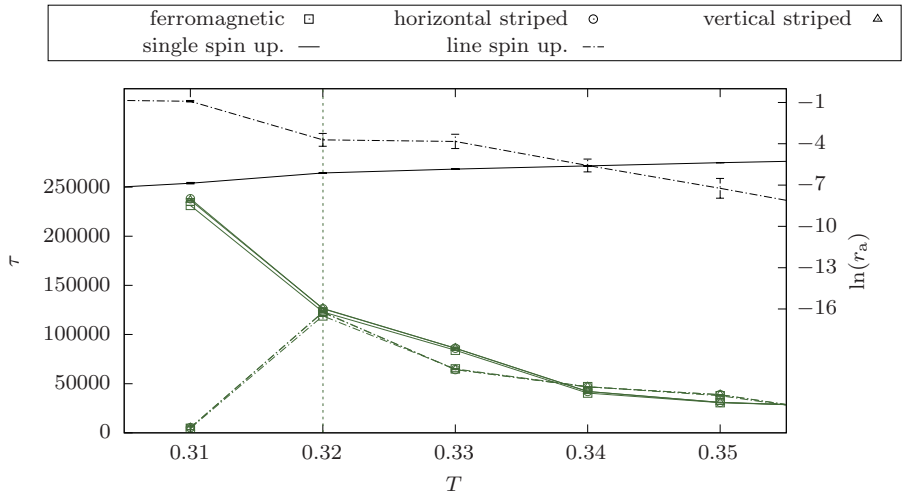

Figure 4.11: This plot combines the relaxation times and acceptance rates as a function of the temperature for $L = 128$. The right vertical axis refers to the values of the relaxation times (green) and the left one to the logarithm of the acceptance rates (black).

In a visual way, this is understandable through the snapshots in Figure 4.12. Both algorithms transit the system in near ground-state at low temperature within a sufficiently large number of sweeps.

However, it is hard to sample ground-state patterns with the single spin

update, originated by the high energy costs of the necessary spin flip sequence resulting in an effectively freezing into an explicit state.

On the other hand, the correct line flips cost no energy, and therefore the simulated system easily transits between ground-states, implying a good ground-state sampling. This point of view is supported by the behavior of the corresponding acceptance rates, Figure 4.5.

Figure 4.12: This graphics shows snapshots for the single and line spin update at $T=0.3$ after $N_{\text{equi}}=5\cdot10^7$ sweeps for a system initialized in a high temperature state with lattice length $L=120$.

5 Conclusion

5.1 Summary

For the equilibrium properties the results and the corresponding discussion of the simulated data lead to the following conclusion. The analysis of the specific heat suggests a peak at the temperature $T_{\max} = 0$ in the thermodynamic limit, and hence the system exhibits no phase transition at a finite temperature. The exponential divergence presumption of the correlation length Ref. [2] could be further supported, Table 4.2. There is no significant behavior of the magnetic observables findable within the considered temperature range.

The dynamical properties of the single spin update depicts highly correlated measurements at low temperatures, resulting from the frustrations. In comparison, the line spin update overcomes these frustrations and samples the low temperature range very well, Figure 4.4. For the quenches into a high temperature state (warming run), a memory effect, being noticeable by the spin autocorrelations remaining in excess, could not be observed for the line spin updates, arguing against a glassy behavior, Figure 4.4. The relaxation times of the low temperature quenches (cooling run) have quite a high value but no singular behavior for the line spin update. This does not fully contradict the glassy behavior. Nevertheless, the findings suggests that the obtained behavior in Ref. [3] is a dynamic effect of the used simulation algorithm. Therefore, the apparent glassiness results perhaps from high frustration, particularly in combination with the single spin update. However, this presumption has to be further verified by continuing studies.

5.2 Outlook

A possible continuing study is a variation of the system under consideration, in particular other boundary conditions e.g. free boundary conditions. Binder et al. [15] mention that a spin glass behavior is highly subjected to boundary conditions. Thus, similar observations could support the glassiness. Another approach is to construct an order parameter in the fashion of Equation (10) with the other ground-states in addition to the ferromagnetic, vertical and horizontal striped ones. However, this could be quite cumbersome in implementations for larger system sizes, caused by a high degeneracy $2^{L+1} - 1$, Section 2.1. With this potential order parameter, studies of its susceptibility appear to be more fruitful than these one associated to a single representative of the ground state.

A Derivatives of the free energy

A.1 Data generation details

This section gives a compiling and execution instruction to reproduce the numerical work of the experiment in Section 4.1. Firstly, the submission folder `submission/` contains four subfolders. The necessary codes are in `generateK/` and `analyzeK/` for the mentioned experiment. All `c++`-codes are compiled with the C++20 standard (`-std=c++20`) and an optimization level two (`-O2`).

Simulation code

The folder `generateK/` includes the files `main.cpp` with the main-function, `system.hpp` with all used declarations and `system.cpp` contains the corresponding definitions. Before compiling, the lines 17-20 of the header file may have to modified for the desired purpose. In line 17 the object-like macro set to `true` correspond to a compiling with the line spin update algorithm and to `false` with the single spin update. The integer in line 18 correspond to the lattice length L. The coupling constants J_1 and J_2 are evaluated by the floating point numbers in lines 19 and 20. A set of six command line arguments must be passed to the resulting executable.

1. PRNG seed as unsigned integer
2. simulation temperature T as floating point number
3. initial state I as character `F` correspond to the ferromagnetic initial state, `H` to the horizontal striped one, `V` to the vertical striped one and `U` or any other character to the uniformly distributed one
4. number of equilibration sweeps N_{equi}
5. number of sweeps for data collection N_{meas}
6. number of sweeps within a subtracting block for the Jackknife method m_J

These arguments are chosen according to the Tables A.1 and A.2 for the considered lattice lengths. The compiled executable generates the folder `L_-_/` (1^{st} gap correspond to L and 2^{nd} one to the initial state) in the current working directory, if the folder does not already exist. In this folder a subfolder is generated corresponding to the chosen T. The entire energy histogram with the magnetization-lists (`entire.txt`) is stored in this folder as well as the N_{meas}/m_J block histograms (`block_.txt`). Furthermore, the final PRNG engine state, the final lattice state, the final values of E, M, M^2,M_s, M_s^2 and the PRNG seed, N_{equi}, N_{meas}, m_J is written in `save.txt` for a possible continuing of the simulation.

L	I	N_{equi}	N_{simu}	N_{jack}
30	U	$2.0 \cdot 10^7$	$5.0 \cdot 10^7$	$5.0 \cdot 10^5$
40	U	$2.0 \cdot 10^7$	$5.0 \cdot 10^7$	$5.0 \cdot 10^5$
50	U	$2.0 \cdot 10^7$	$5.0 \cdot 10^7$	$5.0 \cdot 10^5$
60	U	$2.0 \cdot 10^7$	$5.0 \cdot 10^7$	$5.0 \cdot 10^5$
70	U	$5.0 \cdot 10^7$	$1.0 \cdot 10^8$	$1.0 \cdot 10^6$
80	U	$5.0 \cdot 10^7$	$1.0 \cdot 10^8$	$1.0 \cdot 10^6$
90	U	$5.0 \cdot 10^7$	$1.0 \cdot 10^8$	$1.0 \cdot 10^6$
100	U	$1.0 \cdot 10^8$	$1.5 \cdot 10^8$	$1.5 \cdot 10^6$
110	U	$1.0 \cdot 10^8$	$1.5 \cdot 10^8$	$1.5 \cdot 10^6$
120	U	$1.0 \cdot 10^8$	$1.5 \cdot 10^8$	$1.5 \cdot 10^6$

Table A.1: This table shows all simulation parameters except for the temperatures and the PRNG seeds.

Data analysis codes

All codes for the data analysis are contained in the folder `analyzeK/` in `submission/`. The executable of `mean.cpp` needs the following two command line arguments.

1. relative path from the current working directory to the target folder `L_-_/` and the corresponding name
2. relative path from the current working directory and name of the output `txt`-file

This executable computes for all temperatures in `L_-_/` the means and errors of the considered observables through the obtained histograms and magnetization lists. Compiling `wham.cpp` results in an executable, generating reweighed data points of the considered observables as a function of T with WHAM. The five command line arguments have to pass for a faultless execution.

1. relative path from the current working directory to the target folder `L_-_/` and the corresponding name
2. relative path from the current working directory and name of the output `txt`-file
3. the lower temperature boundary T_{min} as floating point number of the reweighing range
4. the upper temperature boundary T_{max} as floating point number of the reweighing range
5. the number of reweighed data points

The executable of `peak.cpp` determines for each temperature in `L_-_/` all the Jackknife histograms corresponding to their block number. The WHAM procedure is only applied to the specific heat, to obtain the maximum of c for

L	(T, seed)
30	$(0.37, 9481)$,$(0.386, 8879)$,$(0.402, 1876)$,$(0.418, 8270)$, $(0.434, 1628)$,$(0.45, 9600)$,$(0.466, 5181)$,$(0.482, 8255)$, $(0.498, 7964)$,$(0.514, 7966)$,$(0.53, 8799)$
40	$(0.35, 3101)$,$(0.36, 6454)$,$(0.37, 2636)$,$(0.38, 3449)$, $(0.39, 4370)$,$(0.4, 3573)$,$(0.41, 2464)$,$(0.42, 9733)$, $(0.43, 6951)$,$(0.44, 9248)$,$(0.45, 404)$
50	$(0.34, 1262)$,$(0.35, 3959)$,$(0.36, 323)$,$(0.37, 7862)$, $(0.38, 3965)$,$(0.39, 9907)$,$(0.4, 4951)$,$(0.41, 353)$, $(0.42, 4764)$,$(0.43, 6756)$,$(0.44, 5063)$
60	$(0.33, 1304)$,$(0.34, 9748)$,$(0.35, 666)$,$(0.36, 7767)$, $(0.37, 6541)$,$(0.38, 6140)$,$(0.39, 4617)$,$(0.4, 848)$, $(0.41, 8426)$,$(0.42, 8597)$,$(0.43, 5430)$
70	$(0.32, 9334)$,$(0.33, 5248)$,$(0.34, 1710)$,$(0.35, 5503)$, $(0.36, 5083)$,$(0.37, 4443)$,$(0.38, 8094)$,$(0.39, 8390)$, $(0.4, 3062)$,$(0.41, 4150)$,$(0.42, 7934)$
80	$(0.32, 5660)$,$(0.326, 478)$,$(0.332, 286)$,$(0.338, 5366)$, $(0.344, 3288)$,$(0.35, 4412)$,$(0.356, 4696)$,$(0.362, 4554)$, $(0.368, 7866)$,$(0.374, 4665)$,$(0.38, 2323)$
90	$(0.32, 849)$,$(0.325, 120)$,$(0.33, 4593)$,$(0.335, 8940)$, $(0.34, 80)$,$(0.345, 8962)$,$(0.35, 4891)$,$(0.355, 3008)$, $(0.36, 115)$,$(0.365, 4401)$,$(0.37, 8335)$
100	$(0.31, 7564)$,$(0.315, 545)$,$(0.32, 7460)$,$(0.325, 6423)$, $(0.33, 819)$,$(0.335, 6148)$,$(0.34, 2233)$,$(0.345, 7)$, $(0.35, 9428)$,$(0.355, 7516)$,$(0.36, 4740)$
110	$(0.31, 9200)$,$(0.314, 9894)$,$(0.319, 5784)$,$(0.323, 6224)$, $(0.328, 3936)$,$(0.332, 4971)$,$(0.337, 6983)$,$(0.341, 672)$, $(0.346, 6819)$,$(0.35, 6636)$
120	$(0.3, 7976)$,$(0.304, 2828)$,$(0.309, 9951)$,$(0.313, 3972)$, $(0.318, 2650)$,$(0.322, 620)$,$(0.327, 2653)$,$(0.331, 3733)$, $(0.336, 3299)$,$(0.34, 1100)$

Table A.2: The chosen temperatures and PRNG seeds are depicted for the considered lattice length.

each block number, displaying on the console. Furthermore, the lattice length, the mean and the error of the peak location is written in the output file. The following set of command line arguments must be passed to the executable.

1. relative path from the current working directory to the target folder `L_-_/` and the corresponding name
2. relative path from the current working directory and name of the output `txt`-file
3. number of Jackknife blocks

4. the lower temperature boundary T_{min} as floating point number of the reweighing range

5. the upper temperature boundary T_{max} as floating point number of the reweighing range

6. the number of reweighed data points

The same output `txt`-file should be chosen while applying this executable on different target folders (different L) or repeating the execution of a target, because the corresponding data will be appended or overwritten in this file. The reweighing temperature ranges are chosen according to the smallest and largest considered temperatures in `L_-_/`, further the number of the reweighed data points is selected such that a temperature precession of 0.000001 is achieved.

A.2 Consistency checks

The implementations mentioned in the previous two sections are qualitatively verified by the specific heat data for $L \in \{50, 80, 100\}$ and $J_2 \in \{-0.3, -0.6\}$. The same procedure depicted in Section 4.1 is applied for these lattice lengths and NNN-interaction constants. For all cases the system is initiated in a high temperature state (`U`) and is equilibrated through $N_{\text{equi}} = 1.0 \cdot 10^6$ sweeps. Afterward, the entire energy histograms and the corresponding magnetization lists are obtained by $N_{\text{meas}} = 5.0 \cdot 10^6$ measurements. For the errors, the subtracting block length is chosen $m_J = 5.0 \cdot 10^4$. The temperatures and PRNG seeds are selected according to Table A.4. The specific heat reference data is extracted from the work of Kalz et al. [1].

The data of the free energy derivatives for $J_2 = -0.3$ is shown in Figure A.1. The simulated specific heat data agrees with the reference values, some deviations in proximity of the maximum are noticeable for $L = 100$, perhaps originated by N_{meas} selected too small. The received peak locations are shown in Table A.3. While lowering the temperature the depicted magnetization per lattice site increases and approaches 1, emphasizing the ferromagnetic ordering of the low temperature phase for $J_2 \in (-1/2, 0]$ mentioned in Section 2.3.

	$J_2 = -0.3$		$J_2 = -0.6$	
L	T_{max}	$c_{V,\text{max}}$	T_{max}	$c_{V,\text{max}}$
50	1.26589(93)	2.073(13)	0.97413(18)	9.105(71)
80	1.2598(45)	2.324(27)	0.97310(21)	14.55(21)
100	1.26022(77)	2.455(30)	0.97242(26)	18.70(48)

Table A.3: The observed peak locations are shown in this table for the considered cases.

The $J_2 = -0.6$ case is illustrated in Figure A.2. The values of the specific heat is in a good agreement with the reference data of Kalz et al. Furthermore, the peak locations and errors are shown in Table A.3 as well. The depicted

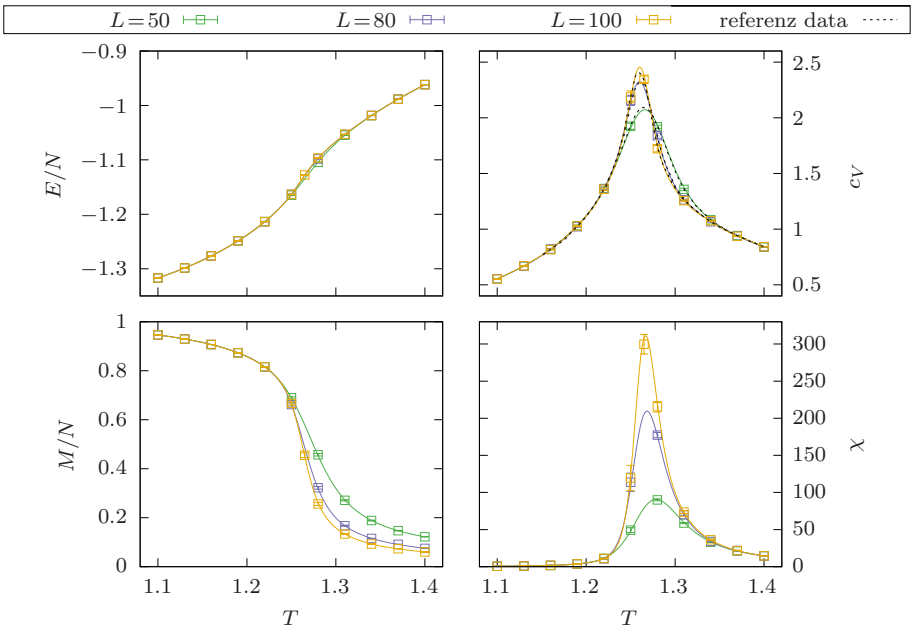

Figure A.1: This plot shows the means and corresponding errors (squares) of the free energy derivatives for $J_2 = -0.3$. The full lines refer to the data obtained by WHAM.

magnetization behaves according to the prediction of a super-antiferromagnetic ordering in the low temperature phase for $J_2 \in (g^*, -1/2)$.

Especially, the vicinity of the specific heat and susceptibility emphasizes phenomenological the kind of the phase transition for the considered J_2. The maximums narrow and grow slowly for $J_2 = -0.3$, presuming a power divergence in the thermodynamic limit (Continuous phase transition), compared to the rapidly narrowing and growing of the peaks for $J_2 = -0.6$, which is an evidence of a δ-function like singularity in the thermodynamic limit (Discontinuous phase transition) [1].

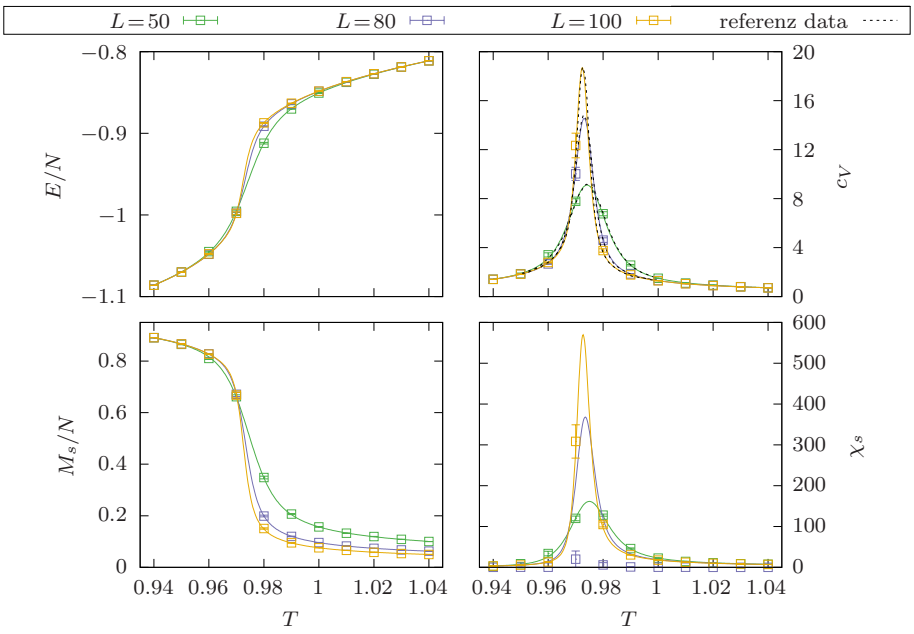

Figure A.2: The free energy derivatives are shown for $J_2 = -0.6$. Particularly, the magnetic observables are depicted for the super-antiferromagnetic case.

$J_2 = -0.3$

L	(T, seed)
50	$(1.1, 9445)$,$(1.13, 3126)$,$(1.16, 7097)$,$(1.19, 4494)$, $(1.22, 6778)$,$(1.25, 3437)$,$(1.28, 3416)$,$(1.31, 9142)$, $(1.34, 1193)$,$(1.37, 6181)$,$(1.4, 7924)$
80	$(1.1, 5089)$,$(1.13, 1936)$,$(1.16, 5560)$,$(1.19, 7161)$, $(1.22, 7240)$,$(1.25, 7910)$,$(1.28, 8669)$,$(1.31, 2216)$, $(1.34, 6146)$,$(1.37, 8672)$,$(1.4, 7208)$
100	$(1.1, 7987)$,$(1.13, 3823)$,$(1.16, 9466)$,$(1.19, 1387)$, $(1.22, 4255)$,$(1.25, 5861)$,$(1.265, 666)$,$(1.28, 3554)$, $(1.31, 736)$,$(1.34, 9762)$,$(1.37, 3708)$,$(1.4, 7651)$

$J_2 = -0.6$

L	(T, seed)
50	$(0.94, 7880)$,$(0.95, 5997)$,$(0.96, 7716)$,$(0.97, 746)$, $(0.98, 3313)$,$(0.99, 9276)$,$(1.0, 247)$,$(1.01, 5423)$, $(1.02, 3587)$,$(1.03, 3602)$,$(1.04, 2052)$
80	$(0.94, 8849)$,$(0.95, 1158)$,$(0.96, 7295)$,$(0.97, 8570)$, $(0.98, 5735)$,$(0.99, 20)$,$(1.0, 2357)$,$(1.01, 9621)$, $(1.02, 4962)$,$(1.03, 4354)$,$(1.04, 5475)$
100	$(0.94, 6845)$,$(0.95, 3487)$,$(0.96, 7288)$,$(0.97, 3574)$, $(0.98, 9363)$,$(0.99, 4849)$,$(1.0, 5107)$,$(1.01, 5831)$, $(1.02, 3572)$,$(1.03, 5922)$,$(1.04, 5875)$

Table A.4: This table depicts the PRNG seed for the corresponding temperatures, lattice lengths and NNN-interaction constants.

B Spin autocorrelation

B.1 Data generation details

In analogy to the experiments of the free energy derivatives, the compiling and execution instruction are presented in the following for the experiments in Section 4.2. The used codes are in the subfolders `generateT/` and `analyzeT/` of the submission folder `submission/`. The `c++`-codes are compiled with the flags `-std=c++20` and `-O2`. The necessary `python`-code requires the `sys`, `numpy` and `scipy` modules.

Simulation code

The `c++`-files associated with the simulation are located in the folder `generateT/`. The file `main.cpp` contains the main-function and the callable (function pointer) for the thread objects. The remaining files `system.hpp` and `system.cpp` includes all declarations and definitions. Perhaps, some lines of the header file has to be modified before compiling. The object like macro in line 19 set to `true` enables the line spin update. The integer and the both floating point numbers in line 20-22 correspond to L, J_1 and J_2. This implementation has the possibility of (trivial) multiple threading. The number of threads is chosen in line 23. The following command line arguments have to pass while starting the execution.

1. PRNG seed as unsigned integer
2. lower boundary of considered temperature range T_{min} as floating point number
3. upper boundary of considered temperature range T_{max} as floating point number
4. step length between two temperatures ΔT as floating point number
5. initial state I as character `F` correspond to the ferromagnetic initial state, `H` to the horizontal striped one, `V` to the vertical striped one and `U` or any other character to the uniformly distributed one
6. number of equilibration sweeps between two temperatures N_{chan}
7. number of sweeps for data collection N_{meas}
8. number of run repeations for the means and errors N_{repe}

The chose arguments are depicted in Table B.1 for the different lattice length and update algorithms. The resulting executable generates the folder `L_-_/` corresponding to the chosen lattice length and initial state as well. In this folder the `txt`-files `T_.txt` are stored, containing the spin autocorrelation functions as function of t_2, associated to the simulated temperatures. Additionally, the means and errors of the acceptance rate as function of T are stored in `acceptance.txt` for the line flip proposals and spin flip proposals.

L	seed	$T_{\min}$	$T_{\max}$	ΔT	I	N_{chan}	N_{meas}	N_{repe}
32	$712, 3730$	0.2	0.5	0.01	`F`	$1.0{\cdot}10^5$	$1.0{\cdot}10^5$	50
64	$4323, 9761$	0.2	0.5	0.01	`F`	$1.0{\cdot}10^5$	$1.0{\cdot}10^5$	50
128	$6577, 1373$	0.2	0.5	0.01	`F`	$1.0{\cdot}10^5$	$1.0{\cdot}10^5$	50
	$4116, 6918$	0.3	0.6	0.01	`U`	$5.0{\cdot}10^6$	$1.0{\cdot}10^5$	4

Table B.1: All the chosen simulation parameters are shown for both update algorithms. The first PRNG seed is associated with the single spin update and the second one to the line spin update.

Data analysis codes

The `python`-code for the data analysis is included in the folder `analyzeT/`. The following parameters/arguments has be chosen in line 8-10 or has to be passed as command line arguments.

1. relative path from the current working directory to the target folder `L_-_/` and the corresponding name
2. lower boundary of considered temperature range $T_{\min}$ as floating point number
3. upper boundary of considered temperature range $T_{\max}$ as floating point number

The code generates in `L_-_/` the `txt`-file `relax.txt` containing the relaxations times as a function of the temperature T for the ferromagnetic, horizontal striped and vertical striped spin autocorrelation functions. Unfortunately, the code works only pretty well for the targets with initial states uniformly distributed (`L_-U/`).

Bibliography

[1] A. Kalz, A. Honecker, S. Fuchs, and T. Pruschke, The European Physical Journal B **65**, 533 (2008).

[2] J. H. Lee, S.-Y. Kim, and J. M. Kim, Phys. Rev. B **109**, 064422 (2024).

[3] R. Timmons and K. De'Bell, Canadian Journal of Physics **96**, 912 (2018).

[4] S. Jin, A. Sen, and A. W. Sandvik, Phys. Rev. Lett. **108**, 045702 (2012).

[5] K. Yoshiyama and K. Hukushima, Phys. Rev. E **108**, 054124 (2023).

[6] C. Fan and F. Y. Wu, Phys. Rev. B **2**, 723 (1970).

[7] L. Landau and E. Lifshitz, *Statistical Physics*, 3rd ed., Vol. 5 (Butterworth-Heinemann, Oxford, 1980).

[8] F. Schwabl, *Statistische Mechanik*, 3rd ed., Springer-Lehrbuch (Springer Berlin, Heidelberg, 2000).

[9] W. Janke, Monte carlo simulations in statistical physics - from basic principles to advanced applications, in *Order, Disorder and Criticality* (World Scientific, 2012) Chap. 3, pp. 93–166.

[10] H. Stanley, *Introduction to Phase Transitions and Critical Phenomena*, International series of monographs on physics (Oxford University Press, 1987).

[11] W. Janke, First-order phase transitions, in *Computer Simulations of Surfaces and Interfaces*, edited by B. Dünweg, D. P. Landau, and A. I. Milchev (Springer Netherlands, Dordrecht, 2003) pp. 111–135.

[12] J. M. Kosterlitz, Journal of Physics C: Solid State Physics **7**, 1046 (1974).

[13] D. P. Landau, Phys. Rev. B **21**, 1285 (1980).

[14] H. Li and L.-P. Yang, Phys. Rev. E **104**, 024118 (2021).

[15] K. Binder and A. P. Young, Rev. Mod. Phys. **58**, 801 (1986).

[16] M. Mézard and G. Parisi, Journal of Physics: Condensed Matter **12**, 6655 (2000).

[17] H. Westfahl, J. Schmalian, and P. G. Wolynes, Phys. Rev. B **64**, 174203 (2001).

[18] U. Kamber, A. Bergman, A. Eich, D. Iuşan, M. Steinbrecher, N. Hauptmann, L. Nordström, M. I. Katsnelson, D. Wegner, O. Eriksson, and A. A. Khajetoorians, Science **368** (2020).

[19] T. R. Kirkpatrick and P. G. Wolynes, Phys. Rev. A **35**, 3072 (1987).

[20] T. R. Kirkpatrick and P. G. Wolynes, Phys. Rev. B **36**, 8552 (1987).

[21] N. Metropolis, A. W. Rosenbluth, M. N. Rosenbluth, A. H. Teller, and E. Teller, The Journal of Chemical Physics **21**, 1087 (1953).

[22] W. Janke, Pseudo random numbers: Generation and quality checks, in *Quantum simulations of complex many body systems*, NIC Series, Vol. 10 (2002) pp. 447–458.

[23] E. Behrends, *Elementare Stochastik*, 1st ed., Springer-Lehrbuch (Springer Fachmedien Wiesbaden, 2013).

[24] P. Bevington and D. Robinson, *Data Reduction and Error Analysis for the Physical Sciences*, 3rd ed. (McGraw-Hill Education, 2003).

[25] J. D. Chodera, W. C. Swope, J. W. Pitera, C. Seok, and K. A. Dill, Journal of Chemical Theory and Computation **3**, 26 (2007).